Journal of Hydrology 635 (2024) 131157

Contents lists available at ScienceDirect

Journal of Hydrology

journal homepage: www.elsevier.com/locate/jhydrol

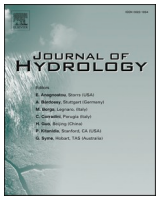

Research papers

Quantifying sediment sources, pathways, and controls on fluvial transport dynamics on James Ross Island, Antarctica

Christopher D. Stringer [a,*], John F. Boyle [b], Filip Hrbáček [c], Kamil Láska [c], Ondřej Nedělčev [d], Jan Kavan [a,e], Michaela Kňažková [c], Jonathan L. Carrivick [a], Duncan J. Quincey [a], Daniel Nývlt [c]

[a] School of Geography and water@leeds, University of Leeds, Woodhouse Lane, Leeds, West Yorkshire LS2 9JT, UK
[b] Department of Geography and Planning, Roxby Building, University of Liverpool, L69 7ZT, UK
[c] Department of Geography, Faculty of Science, Masaryk University, Kotlářská 2, 611 37 Brno, Czech Republic
[d] Charles University, Faculty of Science, Department of Physical Geography and Geoecology, Albertov 6, 128 00 Praha, Czech Republic
[e] Alfred Jahn Cold Regions Research Centre, Institute of Geography and Regional Development, University of Wroclaw, 50-137 Wroclaw, Poland

ARTICLE INFO

This manuscript was handled by Marco Borga, Editor-in-Chief, with the assistance of Edward Park, Associate Editor.

Keywords:
Antarctica
Fluvial sediment
Bedload provenance
Proglacial rivers

ABSTRACT

Proglacial regions are enlarging across the Antarctic Peninsula as glaciers recede in a warming climate. However, despite the increasing importance of proglacial regions as sediment sources within cold environments, very few studies have considered fluvial sediment dynamics in polar settings and spatio-temporal variability in sediment delivery to the oceans has yet to be unravelled. In this study, we show how air temperature, precipitation, and ground conditions combine to control sediment loads in two catchments on James Ross Island, Antarctica. We estimate that the sediment load for the Bohemian Stream and Algal Stream over the 50 day study period, the average sediment load was 1.18 ± 0.63 t km^{-2} d^{-1} and 1.73 ± 1.02 t km^{-2} d^{-1}, respectively. Both catchments show some sensitivity to changes in precipitation and air temperature, but the Algal catchment also shows some sensitivity to active layer thaw. The downstream changes in sediment provenance are controlled by underlying lithology, while differences in sediment load peaks between the two catchments appear to be primarily due to differing glacier and snowfield coverage. This identification of the controls on sediment load in this sub-polar environment provides insight into how other fluvial systems across the Antarctic Peninsula could respond as glaciers recede in a warming climate.

1. Introduction

Rivers are the primary transporter of sediment in proglacial regions (Overeem et al., 2017) and they are shaped by the interplay of glacial meltwater that erodes, transports, and deposits sediment, as well as hillslope activity that provides new sediment to the system during mass transport events. In a warming climate, both sets of processes result in greater sediment discharge, provided peak water (Huss and Hock, 2018) has not yet been reached (Ballantyne, 2008; Carrivick et al., 2018; Staines et al., 2015). Permafrost underlies an extensive part of these proglacial regions, particularly in sub-polar environments, and permafrost-affected soils (active layer) can be an additional source of water and sediment when ground temperatures are above freezing; particularly in catchments with limited glacier cover (Costa et al., 2018; Humlum et al., 2003; Łepkowska and Stachnik, 2018).

Until the start of the 21st century, the Antarctic Peninsula (AP) was one of the most rapidly warming places on Earth (Vaughan et al., 2003; Bentley et al., 2009; Carrivick et al., 2012; Mulvaney et al., 2012; Oliva et al., 2016). Despite a break in this trend, ice masses throughout the AP region have receded at enhanced rates and will continue to do so as air temperatures rise again (Carrasco et al., 2021; Engel et al., 2023). Consequently, some of Antarctica's proglacial regions are expanding along with their permafrost-affected soils, as both land and marine-terminating glaciers recede with a warming climate (Cook et al., 2016; Lee et al., 2017; Oliva and Ruiz-Fernández, 2015).

Glacier recession and enlargement of proglacial regions affect the quantity, spatio-temporal pattern and composition of sediment discharged from Antarctica's rivers and hence the diversity of aquatic life present in its seas, lakes and rivers (Gonçalves et al., 2022). Benthic communities are especially sensitive to change (Friedlander et al., 2020) and suspended sediment in particular has wide-ranging impacts including on the feeding behaviour, reproductive success, and growth of

* Corresponding author.
E-mail address: gycds@leeds.ac.uk (C.D. Stringer).

https://doi.org/10.1016/j.jhydrol.2024.131157
Received 24 November 2023; Received in revised form 5 March 2024; Accepted 16 March 2024
Available online 16 April 2024

organisms (Hodson et al., 2017). Specifically, increased water turbidity reduces photosynthesis and can physically damage small organisms and affect carbon sequestration (Cloern, 1987; García-Rodríguez et al., 2021).

Despite the importance of proglacial regions as sediment sources in sub-polar environments (e.g. Syvitski, 2002; Staines et al., 2015; Overeem et al., 2017), studies from the Southern Hemisphere are sparse. Of the studies that do consider rivers in Antarctica (e.g. Chinn and Mason, 2016; Kavan et al., 2017, 2023), none explored the spatio-temporal variability in sediment delivery or have compiled a comprehensive source-to-sink description of sediment transportation.

To address this, our study aims to take a holistic approach to consider sediment production and transportation in two largely deglaciated catchments, from source to sink. The low areal coverage of glacier ice in these catchments is unusual in an Antarctic context and therefore provides an insight into what many other catchments may look like in the

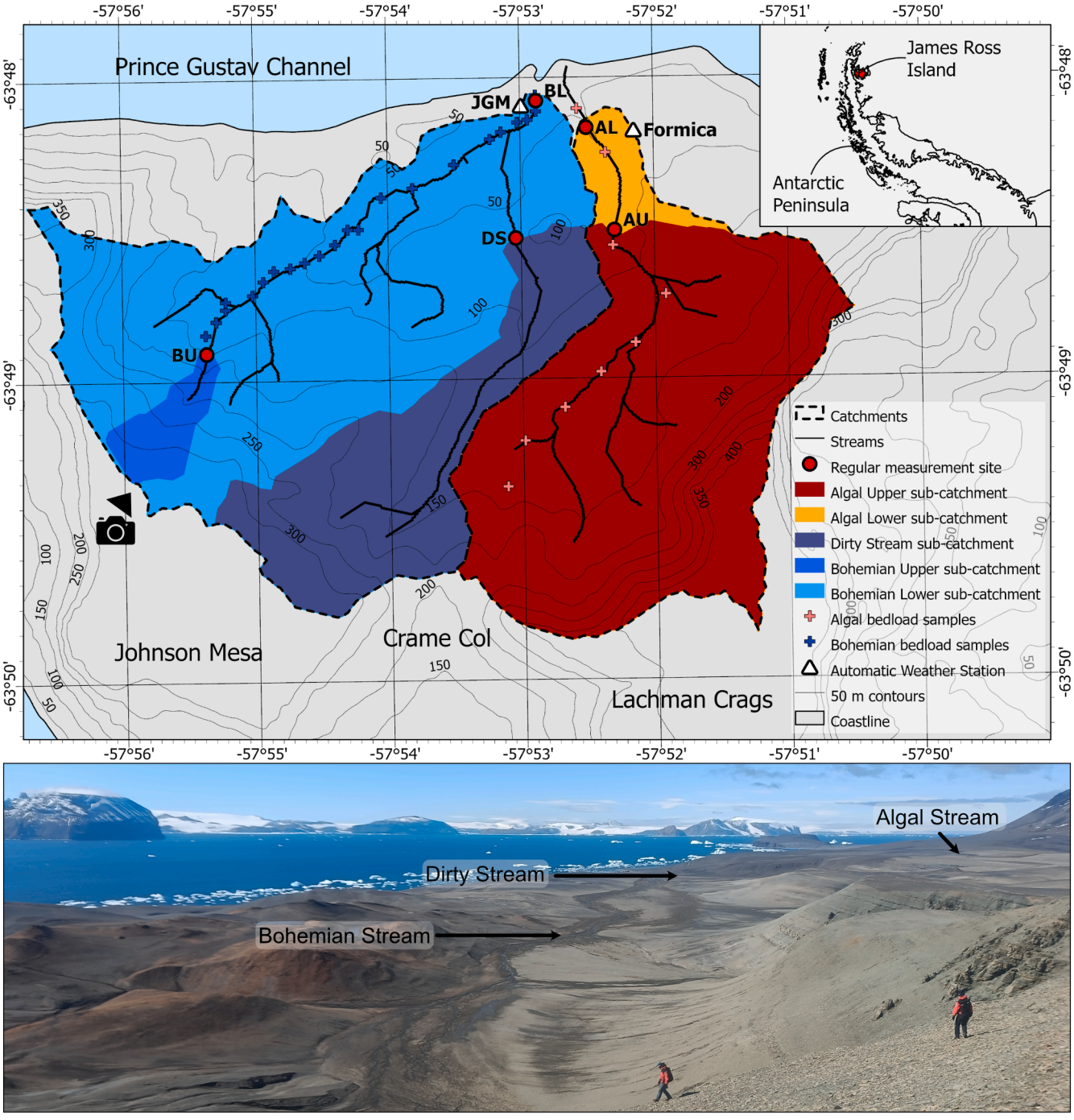

Fig. 1. Location of study sites on James Ross Island, Antarctic Peninsula. River channel and catchments were extracted using the flow accumulation and watershed tools in ArcGIS Pro using the REMA DSM (Howat et al., 2019); some very small channels are not delimited. Coastlines and map of Antarctica are from Gerrish et al. (2020), contours are from the Czech Geological Survey (2009). NB: JGM = Johann Gregor Mendel Station. Photo was taken by CS on the slopes of Johnson Mesa, as highlighted on the map, looking north-east. BL = Bohemian Lower (sub catchment = 6.7 km^2); BU = Bohemian Upper (sub catchment = 0.3 km^2); DS = Dirty Stream (sub catchment = 2.0 km^2); AL = Algal Lower (sub catchment = 4.5 km^2); AU = Algal Upper (sub catchment = 4.2 km^2).

future as glaciers recede. We took hydrological, sedimentological, and geochemical measurements and have analysed them in the context of meteorological and active layer observations to investigate the: **i)** transport of water and sediment in two Antarctic catchments; **ii)** the source of sediments in the catchments.

1.1. Study site

1.1.1. Location and climate

James Ross Island is situated within the James Ross Archipelago, off the northeast coast of the Antarctic Peninsula; across the Prince Gustav Channel from the Trinity Peninsula. It has a semi-arid polar continental climate, with a mean annual air temperature of −6.7 °C in coastal regions (Kaplan Pastíriková et al., 2023), and −9.0 °C in areas of high elevation (Ambrozova et al., 2019). Mean annual precipitation is

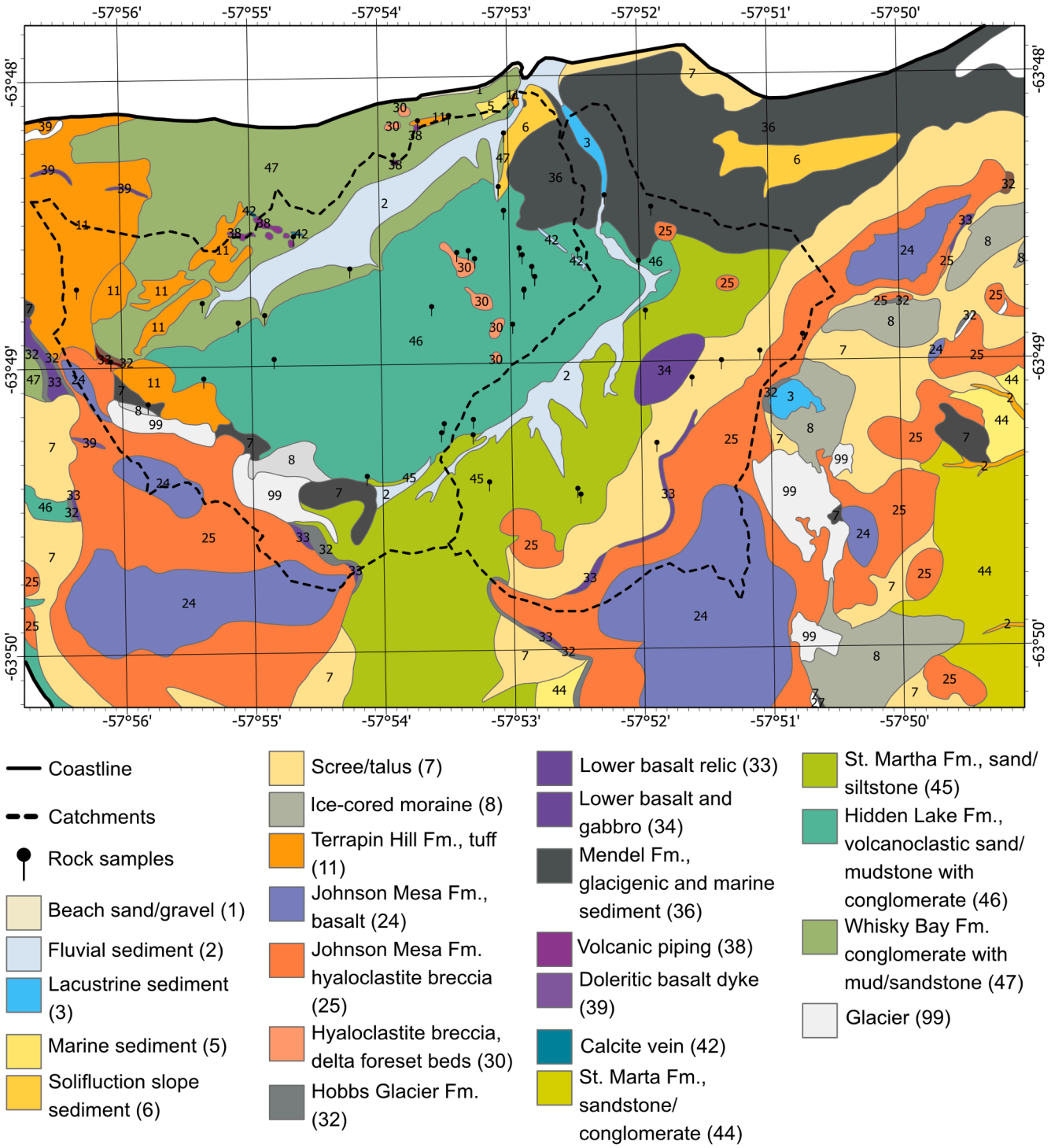

Fig. 2. Geological map of the Algal and Bohemian Stream catchments, based on Czech Geological Survey map (Mlčoch et al., 2020). The location of rock samples collected is also displayed.

estimated at between 400 and 700 mm of water equivalent (Palerme et al., 2017). Snow cover observations at the Johann Gregor Mendel Czech Antarctic Station (Czech Antarctic Research Programme, hereafter referred to as JGM) indicate considerable inter-annual variability in the snowfall but with a snow depth rarely exceeding 0.35 m (Hrbáček et al., 2021).

The river catchments we have studied (Bohemian Stream catchment and Algal Stream catchment) are located close to JGM on the Ulu Peninsula of James Ross Island (Fig. 1). The Ulu Peninsula experienced a period of rapid ice-sheet surface lowering, coincident with the initiation of the Prince Gustav Ice Stream after ~18 ka and a transition from a thick cold-based ice sheet to a warm-based active deglaciation (Glasser et al., 2014), with the lower elevation areas becoming deglaciated ~12.9 ka (Nývlt et al., 2014). Throughout the late Holocene, several small glaciers re-advanced from cirques on the sides of mesas (Carrivick et al., 2012) and today the Ulu Peninsula is the second largest deglaciating terrain area in Antarctica, behind the McMurdo Dry Valleys. Both catchments sit within a crescent of uplands; to the east, this is Lachman Crags (408 m a.s.l.) and to the west, this is Johnson Mesa (323 m a.s.l), these two prominent features meet at Crame Col to the south (178 m a.s.l.). The Bohemian Stream is a braided river that flows towards the east with its source in the upland region of Johnson Mesa. The Dirty Stream, flowing towards the north, is also an important water and sediment source (Sroková and Nývlt, 2021) to the Bohemian Stream's total sediment budget and is its largest tributary. The Algal Stream catchment is separated from the Bohemian Stream catchment by a small ridge that runs parallel to the Dirty Stream. The upper section of the main river channel mostly flows parallel to the Bohemian Stream, while the lower section bends to flow towards the north.

1.1.2. Geological setting

Both catchments predominantly lie on Cretaceous marine strata (Fig. 2) composed of mudstones, sandstones and conglomerates (Ineson et al., 1986; Mlčoch et al., 2020). The Cretaceous sediments in the Bohemian catchment are composed of more conglomerate and coarse-grained sandstones in comparison to the finer-grained sandstones and mudstones within the Algal catchment. Parts of both catchments are underlain by Neogene igneous rocks, which are primarily hyaloclastite breccias, tuffs, and subaerial basalts (Mlčoch et al., 2020; Smellie et al., 2008). While the upland regions of both catchments contain siliciclastic and volcanoclastic sediments (Košler et al., 2009), they are finer-grained in the Algal catchment (Mlčoch et al., 2020; Nehyba and Nývlt, 2014). The lower reaches of both catchments are composed of clast-rich diamictites of Miocene to Pliocene age (Davies et al., 2013; Nývlt et al., 2011).

2. Methods and materials

2.1. Stream monitoring

We measured river water discharge and suspended sediment load at five "regular measurement sites" (Fig. 1, supplementary data files SI 1a). These five sites were chosen to capture the water and sediment movement of the upper and lower sections of the Bohemian Stream and the Algal Stream rivers, as well as the influence of a major tributary to the Bohemian Stream; the Dirty Stream. The lower measurement sites (Bohemian Lower: BL, and Algal Lower: AL) were placed at stable cross sections previously used for river measurements by Kavan et al. (2017) and Kavan (2021). We also made new sampling sites in the upper reaches of the Algal Stream (Algal Upper: AU), the Bohemian Stream (Bohemian Upper: BU) and close to the confluence of the Bohemian and Dirty Streams (Dirty Stream: DS). The Dirty Stream site was chosen as the point closest to the Bohemian Stream confluence with a stable cross section. The Algal Upper and Bohemian Upper sites represent the point furthest upstream with a stable cross section. At each of these sites, we measured river water discharge and suspended sediment concentration (SSC) at six-hour intervals for 24 h every two weeks for the duration of the expedition (8 weeks total study time). This resulted in 20 measurements from each of our sites over the course of the season, except for the Bohemian Upper site, which was frozen on two of the visits. Additionally, we took automatic discharge measurements every 10 min at the AL and BL catchment outlet sites (at the AL and BL regular measurement sites, Fig. 1).

2.1.1. River water discharge

We used a SonTek FlowTracker 2 handheld Acoustic Doppler Velocimeter to measure the discharge of the streams at each of our sites (supplementary data files, SI 2a). We recorded the width of the active stream for each measurement and recorded the depth and velocity of the streams approximately every 200 mm, though this varied depending on the stream flow and channel width. This equipment also generated an error assessment of each discharge measurement, which is a function of the variability in velocity and pressure in the equipment's readings. The median uncertainty was 0.001 m^3/s.

2.1.2. Suspended sediment concentration

Immediately after measuring discharge, we took a grab sample of water from the centre of the channel in a 220 ml bottle to measure SSC. We pre-weighed these samples in the laboratory of JGM to calculate the total mass of water and sediment in each of the bottles at a precision of 0.01 g. From this, we could calculate the volume of water in each bottle. Using pre-weighed Whatman Grade 6 filters (3 μm), we used a vacuum to filter our samples and dried them in a SNOL 120/300 LSN11 drier at 80 °C for two hours. We then weighed the dried sample at a precision of 0.0001 g and calculated the concentration of suspended sediment (supplementary data files, SI 2a). Median SSC uncertainty was 55 mg l^{-1}. Since many of the uncertainties are fixed, this means that some small SSC measurements are proportionally associated with very high uncertainties.

2.1.3. Continuous discharge

To derive a continuous record of catchment outlet river water discharge (supplementary data files, SI 2b), we continuously measured hydrostatic pressure using a sensor DipperLog F100/M30 (accuracy of ± 0.05 %; Heron Instruments) in a stable profile at the AL (n = 8) and BL (n = 10) regular measurement sites (Kavan et al., 2017; Kavan, 2021). We adjusted these hydrostatic measurements for local air pressure (TMAG 518 N4H barometer (accuracy ± 0.5 hPa; CRESSTO, CZ) to derive water depth and from that computed river water discharge using a stage-discharge rating curve (supplementary data files SI 2c) constructed using manual river water discharge measurements that were independently collected over the course of the season using a SonTek FlowTracker. We used a power law relationship, following the methods of Kavan et al. (2017), and Kavan (2021). This resulted in a Root Mean Squared Error (RMSE) of 0.04 m^3/s for AL (Fig. 3A) and 0.03 m^3/s for BL (Fig. 3B), equivalent to a mean uncertainty of 21 % and 15 % respectively. Discharge measurements used in these calculations were associated with an uncertainty of 14.8 % (BL) and 11.7 % (AL), respectively.

2.1.4. Continuous suspended sediment concentration

A continuous record of suspended sediment concentration (supplementary data files, SI 2b) was derived from a sediment rating curve (Kavan et al., 2017; Kavan, 2021) that was constructed using the derived discharge values (described in 2.1.3), and the SSC samples we manually collected (see section 2.1.2), For the AL site (n = 18), RMSE = 590 mg l^{-1}, and for the BL site (n = 13), RMSE = 820 mg l^{-1} (Fig. 3D) (supplementary data files SI 2c). This is equivalent to a mean uncertainty of 56 % and 51 % respectively.

Herein, continuous measurements are described by "SSC", but where inter-site analysis is presented, we use "sediment load" to account for differences in catchment area. We have defined sediment load as the mass of suspended sediment transported through a point in a given

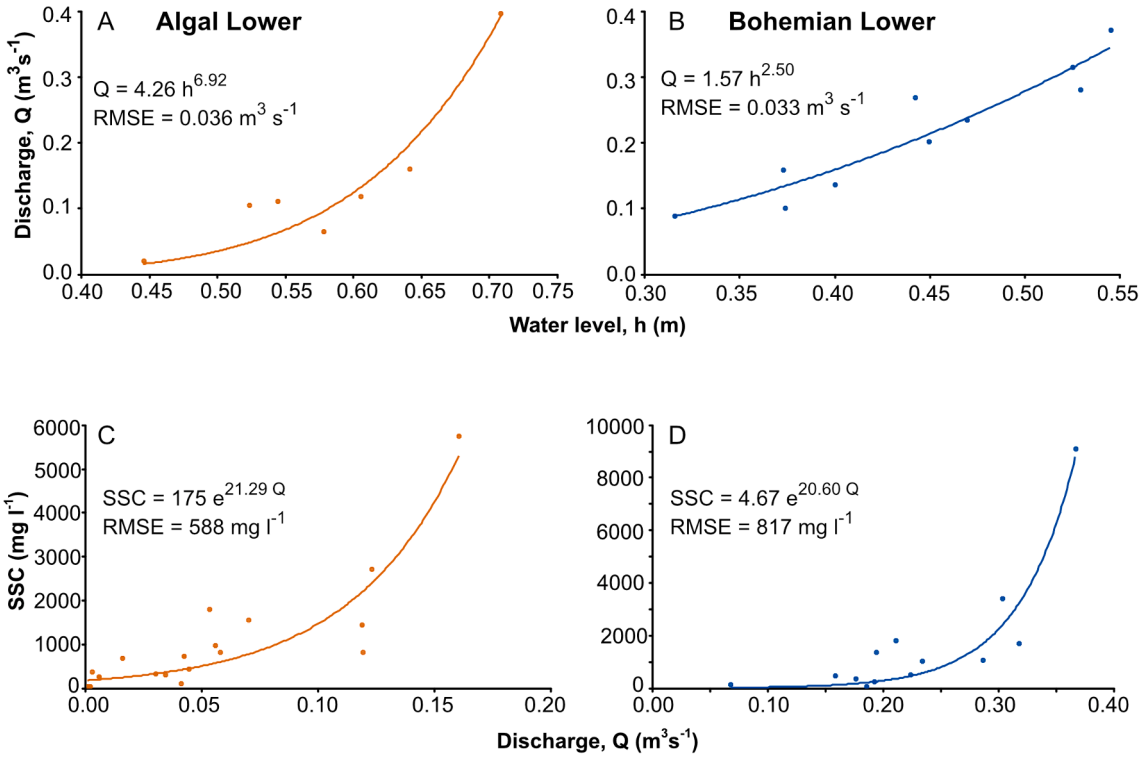

Fig. 3. Rating curves showing A) stage-discharge relationship for the Algal Lower; B) stage-discharge relationship for the Bohemian Lower; C) Discharge and suspended sediment concentration (SSC) relationship for the Algal Lower; D) Discharge and suspended sediment concentration relationship for the Bohemian Lower.

period, per square kilometre of its catchment area and it was calculated by calculating the sediment transported at a point per minute and dividing it by the catchment area (supplementary data files SI 2a); the catchment area is derived using the sub-catchments in Fig. 1 (BL = 6.7 km^2; BU = 0.3 km^2; DS = 2.0 km^2; AL = 4.5 km^2; AU = Algal Upper = 4.2 km^2). This is to ensure that any inter-site comparison is adjusted for differences in the catchment area. Suspended sediment processing was associated with an uncertainty of 4.2 % (BL) and 2.3 % (AL).

2.2. Samples of bed material and rocks

Samples of bed material with clasts up to gravel size were taken from the centre of the channel in the Bohemian Stream and the Algal Stream (Fig. 1), for geochemical analysis. These were collected at ~ 100 m intervals (21 samples) in the Bohemian Stream. For logistical reasons, the sampling interval was set at ~ 300 m intervals along the Algal Stream (9 samples). Rock samples were sampled from each lithological unit in both catchments (Bohemian catchment: 28, Algal catchment: 15), as informed by the geological map of the region (Mlčoch et al., 2020), consistent with the strategy used in previous studies in this region (Kavan et al., 2017; Sroková and Nývlt, 2021). Samples largely constituted solid samples of bedrock, but in some cases were samples of surface sediments (i.e. regolith). Samples taken in the field were interpreted and their composition confirmed, to ensure there were no errors in the geological map (Supplementary Data Files SI 5a).

2.3. Meteorological observations

We used air temperature and precipitation data (supplementary data files SI 3) from the automatic weather station located near JGM. Air temperature was measured using a Pt100/A resistance thermometer (accuracy of ± 0.15 °C) with a built-in EMS33H probe (EMS Brno, Czech Republic) installed at 2 m above the ground in a multi-plate radiation screen. Ground-based measurement of precipitation was carried out using a Thies laser precipitation monitor (Adolf Thies GmbH & Co., Germany) enabling both quantitative precipitation estimation (rain/snow rates and totals) and the detection of different types, i.e. drizzle, rain, hail, snow, and sleet. For the analysis, instantaneous 30-min and mean daily air temperatures were used, while daily totals and prevailing types of precipitation were calculated from 1-min observations.

2.4. Active layer measurements

We used the ground thermal regime data from JGM and Formica meteorological stations to represent the catchments of the Bohemian Stream and Algal Stream, respectively (Fig. 1, supplementary data files SI 3). At both sites, the ground temperature measurement was conducted in a 2 m deep profile with measurements collected at selected depths (0.05, 0.5, 0.75, 1 m) using resistance thermometer detectors (Pt100/8, accuracy +- 0.15 °C), which measured and stored data every 30 min. For our analysis, we used daily means of near-surface ground temperature measured at a depth of 0.05 m. Furthermore, we studied the detailed daily course of the 0.05 m temperature on selected days. The data from deeper parts of the profile (0.50 m, 0.75 m, 1 m) were used for interpolation of the daily position of the 0 °C isotherm (e.g. Hrbáček et al., 2021) and we derived the daily thaw rate as a difference of the thaw depth between two consecutive days.

2.5. Provenance of bed material

2.5.1. Sample preparation

As described, bed material was sieved to collect the < 2 mm fraction. This **a)** improved the ease with which they could be manually crushed with an agate pestle and mortar, and; **b)** ensured the most mobile fraction of sediments were sampled. We also crushed fissile rock samples with a pestle and mortar. For more resistant lithologies, we used a masonry drill bit with a high Moh's hardness and collected the dust produced for analysis. Crushing samples reduced the impact of grain size, a major component of uncertainty in sediment provenance studies, and ensured they were homogenised (Collins et al., 2020). The grain size of

individual samples can be found in the supplementary data files (supplementary data files SI 4).

2.5.2. Measurements

A complete analysis of provenance can be achieved by using both XRF and infrared analysis of chemical and mineralogical characteristics, respectively. We measured the X-ray fluorescence (XRF) with a ThermoFisher Scientific Niton XL5 Plus Handheld XRF Analyzer using the mining setting and took three 120-second measurements of each bed material and rock sample (supplementary data files, SI 5a). We measured suspended sediment samples for 160 s. To calibrate the equipment and validate our readings, we measured a standard sample on any day we took a measurement.

We used a Spectral Evolution PSR + 3500 spectrometer with a fibre optic probe to measure infrared reflectance (supplementary data files, SI 5b). Each sample was measured three times and a white reflectance standard was also measured before every measurement to calibrate the equipment and validate our readings.

All bed material and rock samples were measured using both techniques. However, most of the suspended sediment samples were too small to measure, and so only 15 (5 Algal Stream catchment, 10 Bohemian Stream catchment) of these samples were measured.

2.5.3. Analysis

Whilst many recent studies have made use of sediment un-mixing models, there are challenges associated with using these on relatively small datasets, which can led to overfitting from the model (Lipp et al., 2021; Zhao et al., 2022). Recent studies (e.g. Shahrestani et al., 2020) have shown that the areal coverage of lithological units is a good indicator of source material. Therefore, we calculated a sub-catchment for the location of each bed material sample using the hydrology tools in ArcGIS Pro (supplementary data files, SI 1b). The proportion of each lithological unit within these sub-catchments was calculated by spatially querying the most recent and digitally available geological map of the region (Mlčoch et al., 2020, Fig. 2), which gave a list of potential source rocks for each sediment sample.

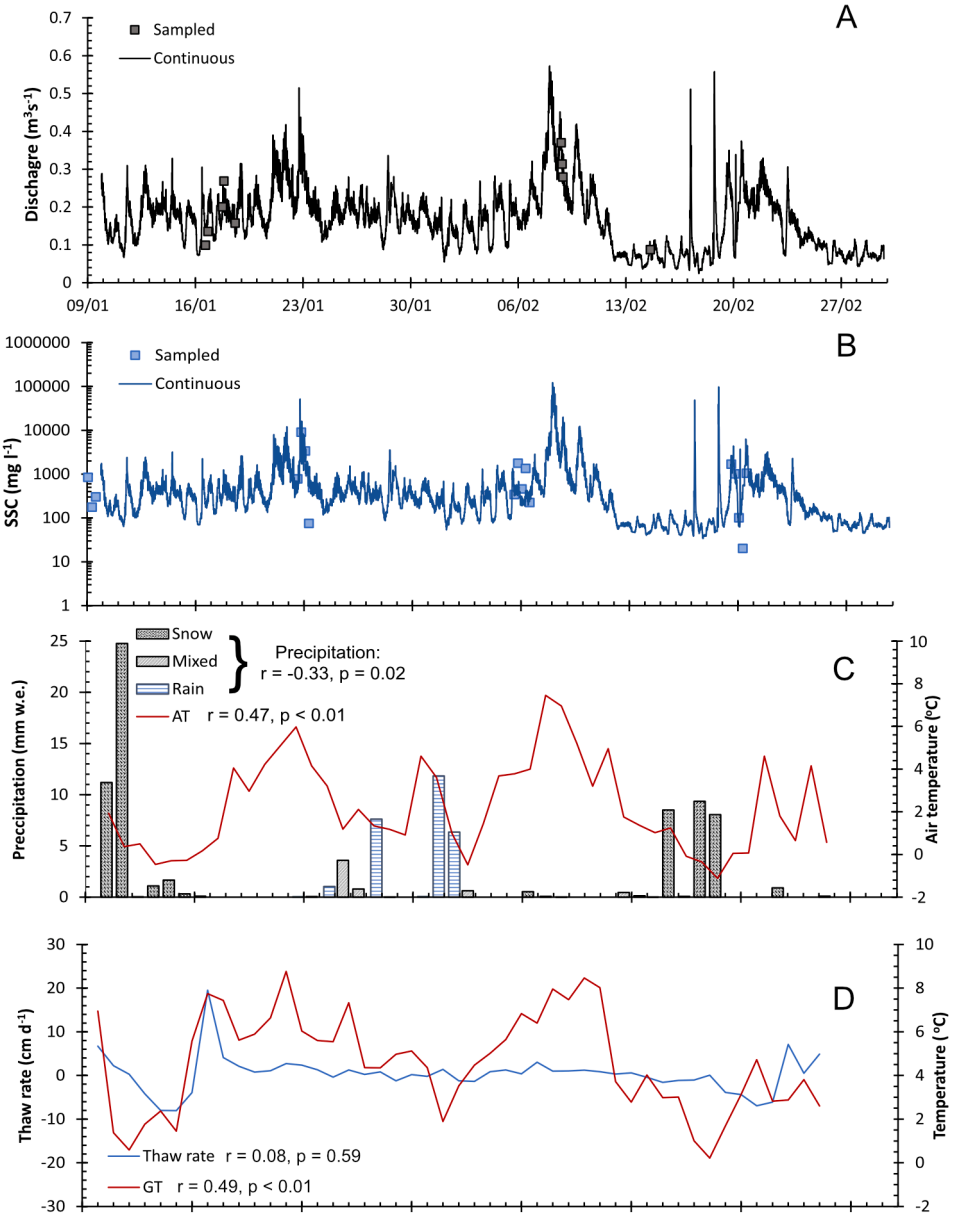

Fig. 4. Data from the Bohemian Lower site, describing: **A)** Discharge; **B)** Suspended sediment concentration; **C)** Precipitation and air temperature (JGM); **D)** Thaw rate (JGM) and ground temperature (JGM). Correlation is between the environmental factor and discharge, with r = correlation coefficient and p = significance.

The infrared spectra were prepared for analysis by taking their first derivative, which has been shown to reduce the impact of unwanted physical information such as grain size on spectra (Russell et al., 2019). This was done using SpectraGryph 1.2 and a Principal Component Analysis was conducted in the Past 4.07b statistical software for each bed material sample. From this, we were able to produce scatter plots between the first three component scores (derived from the PCA correlation matrix) of each bed material sample and the proportion of each geological unit within its sub-catchment. We investigated the relationship between these two variables and conducted a Spearman's Rank correlation analysis on any relationship showing an $R^2 > 0.5$. Any lithology showing a significant correlation ($p < 0.05$) was then considered as an important source rock for stream bed material. The justification for this correlation analysis was that if a unit is deemed to be an important source rock, then its contribution to sediment composition should increase in line with its proportion of the catchment area. We complemented this analysis of infrared by looking at the similarity between the chemical composition of sediment samples and important source rocks.

3. Results

3.1. Suspended sediment export and variability

3.1.1. Temporal variability

The river water discharge (Fig. 4A) and SSC (Fig. 4B) from the Bohemian catchment at the BL site displayed three broad peaks over the course of the study period. The first of these occurred between 21 January and 24 January, with a maximum discharge of 0.51 m^3s^{-1} and a corresponding SSC of 51,837 mgl^{-1} at 17:54 (UCT) on 22 January. We observed in the field that this maximum coincided with a large snowmelt event, during which the snow that fell on 10 January and 11 January (totalling 36 mm w.e. at JGM, Fig. 4C) melted in the upland regions of the catchment, as both air and ground temperature increased (Fig. 4C,

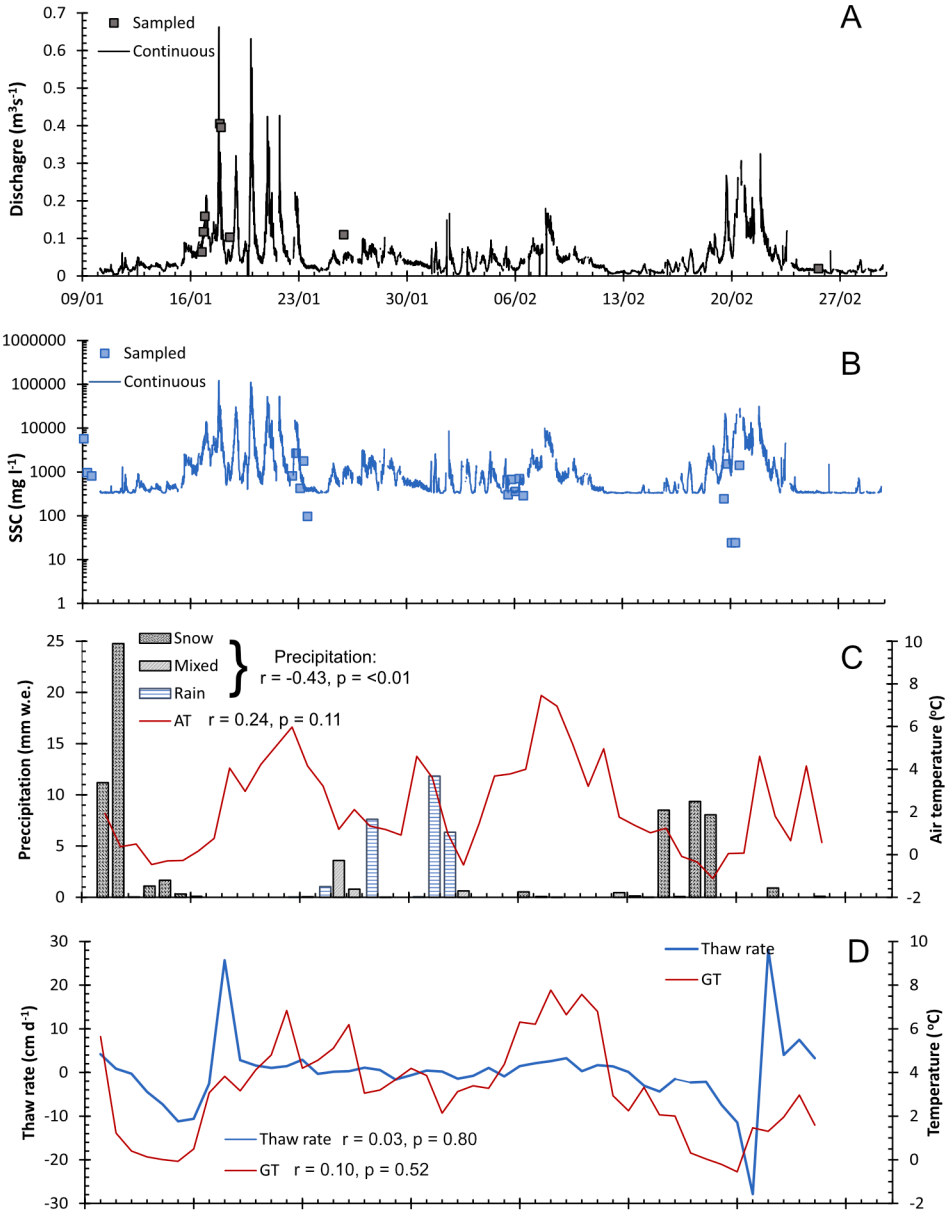

Fig. 5. Data from the Algal Lower site, describing: **A)** Discharge (collected every 10 min); **B)** Suspended sediment concentration (calculated by rating curve from discharge); **C)** Precipitation and air temperature (JGM); **D)** Thaw rate (JGM) and ground temperature (JGM). NB: Correlation is between the environmental factor and discharge with r = correlation coefficient and p = significance.

D). Discharge and SSC peaked again between 7 February and 11 February (Fig. 4A, B), to a maximum discharge of 0.57 m^3s^{-1} and SSC of 122,980 mg l^{-1} at 01:04 on 8 February. This was coincident with rising air and ground temperatures (Fig. 4C, D), air temperature peaked on 7 February with a mean temperature of 7.5 °C (rising from 4.0 °C on the preceding day), and ground temperature increased to 8.0 °C on 8 February. A third peak in discharge and SSC (Fig. 4A, B) occurred between 19 February and 23 February (maximum 0.37 m^3s^{-1} at 12:14 on 20 February, and an SSC = 6334 mgl^{-1}), although this broad peak was preceded by two short-duration peaks in discharge (0.51 m^3s^{-1} and 0.55 m^3s^{-1}) and SSC (49,234 mgl^{-1} and 98,143 mgl^{-1}). These two short-duration peaks are coincident with snowfall (Fig. 4C). The broad peak corresponded with rising air and ground temperatures following a snowfall in the preceding days, with air temperatures rising from 0.1 °C on 20 February to 4.6 °C on 21/2, and ground temperature rising from 3.1 °C to 4.7 °C. Discharge at the BL site has a positive correlation with air temperature ($r = 0.47$, $p > 0.01$, Spearman's Rank) and ground temperature ($r = 0.53$, $p > 0.01$), as well as a weak negative correlation with precipitation ($r = -0.33$, $p = 0.02$) (Fig. 4D). There is no clear relationship between active layer thaw rate and discharge in the Bohemian catchment ($r = 0.08$, $p = 0.59$). According to cross-correlation analysis, there is a possible correlation on a lag time of 7 days, though this is a weak negative relationship.

There were two major peaks in river water discharge and SSC from the Algal catchment at the AL site (Fig. 5A, B), between 16/01 and 24/01. The rising limb of the first peak in the Algal Stream occurred earlier in the Algal Stream than in the Bohemian Stream. During this period, a maximum discharge of 0.66 m^3s^{-1} and SSC of 122,270 mgl^{-1} was reached at 20:16 on 17 January. This maximum discharge was coincident with an increase in thaw rate (Fig. 5D), which peaked at a value of 25.7 cmd^{-1} (i.e. the active layer thawed and became thicker), and an increase in air temperature (to 4.0 °C), on 18 January. A second peak occurred later in the season, between 18 February and 23 February, with a maximum water discharge of 0.33 m^3s^{-1} at 20:26 and SSC of 31,480 mgl^{-1} on 21 February. This second peak largely coincided with an increase in discharge in the Bohemian catchment and is similarly coincident with rising temperatures following a snowfall event (Fig. 5C). Unlike the Bohemian catchment, discharge in the Algal Stream shows no clear correlation with any environmental factor that we measured. There is an insignificant, slight positive relationship with air temperature ($r = 0.24$, $p = 0.11$), and a negative relationship with precipitation ($r = -0.43$, $p = 0.01$). There is no correlation between thaw rate and discharge ($r = 0.03$, $p = 0.80$), though an increase in thaw rate does coincide with a large discharge between 16 February and 24 February. Similar to the Bohemian catchment, there is a possible lag time of 5 to 6 days, though this is a weak negative relationship.

Over the course of the study period, suspended sediment was exported from the Bohemian Stream at an average rate of 235 t $month^{-1}$ and the Algal Stream at 236 t $month^{-1}$. For the 50 day study period, and with a calculated area of 6.7 km^2 for the Bohemian Stream catchment and 4.5 km^2 for the Algal Stream catchment, this gives an estimated suspended sediment load of 1.18 ± 0.63 t km^{-2} d^{-1} and 1.73 ± 1.02 t km^{-2} d^{-1}.

3.1.2. *Spatio-temporal variability*

Daily peak air temperatures were typically recorded at ~ 16:00 UTC and this coincides with peak sediment load across all sites (Fig. 6). On 22–23 January, we measured the highest mean daily sediment load values across all three Bohemian catchment sites (BL = 14,039 kg km^{-2} d^{-1}, BU = 545,723 kg km^{-2} d^{-1}, DS = 19,083 kg km^{-2} d^{-1}), whereas the peak mean sediment load of the Algal catchment (AL = 17,558 kg km^{-2} d^{-1}, AU = 11,465 kg km^{-2} d^{-1}) fell on 8–9 January (Fig. 6). The final measurement date (19–20 February) saw particularly low specific sediment load values across both catchments, with the minimum individual sediment load for the entire measurement period being measured on this day (AL = 1.61 x 10^{-4} kg km^{-2} min^{-1}, AU = 0.00 kg km^{-2} min^{-1}, BL = 3.68 x 10^{-5} kg km^{-2} min^{-1}, DS = 9.01 x 10^{-4} kg km^{-2} min^{-1}). This coincided with sub-zero air temperatures and some parts of the stream (notably AU) being frozen; though there was a very slow flow of water below the frozen surface (resulting in a very low SSC measurement). We typically recorded higher sediment loads at the Bohemian catchment sites, especially at the lower sites (median values for the entire measurement period were: AL = 0.51 kg km^{-2} min^{-1}, AU = 0.37 kg km^{-2} min^{-1}, BL = 0.66 kg km^{-2} min^{-1}, DS = 0.45 kg km^{-2} min^{-1}, BU = 0.04

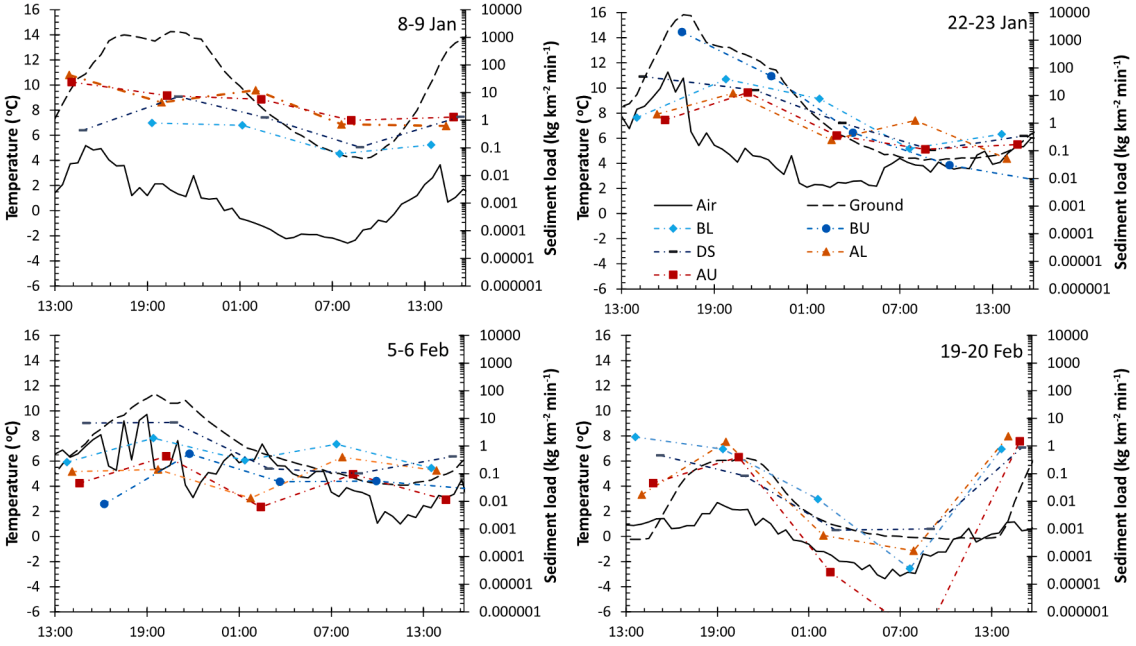

Fig. 6. Specific sediment load measurements from the regular measurement sites for each 24 h measurement period. Plots of air and ground temperature (5 cm depth) collected from the Mendel weather station (10 m a.s.l) are also presented. NB: BL = Bohemian Lower; BU = Bohemian Upper DS = Dirty Stream; AL = Algal Lower; AU = Algal Upper. NB: Median sediment load uncertainty was 18 %, (0.07 kg/min/km2). Much of the errors were fixed, relating to instrument and DEM precision, therefore smaller load values have a higher % uncertainty. All times are in UTC.

kg km^{-2} min^{-1}) with the notable exception of the 8–9 January period, when Algal catchment measurements were highest (median values for this day AL = 4.41 kg km^{-2} min^{-1}, AU = kg km^{-2} min^{-1}, BL = 0.66 kg/min/km^2, DS = 1.25 kg km^{-2} min^{-1}, BU = 0.00 kg km^{-2} min^{-1}). In both catchments, the lower sites have the largest sediment loads, with the Dirty Stream appearing to be a major contributor of sediment to the Bohemian Stream. It should be noted that there are times in both catchments when the specific sediment load is higher in the upper parts/tributaries than in the outflow. The median sediment load uncertainty was 0.07 kg km^{-2} min^{-1}. Most of the errors were fixed, relating to the instrument and DEM precision.

3.2. Provenance of bed material

Possible sources of the Bohemian Stream's bed material are marine sediment (Holocene age), solifluction slope sediments, hyaloclastite breccia, Mendel Fm. (glacigenic, glaciomarine, and marine sediments), St. Marta Fm. (sandstone) and Whisky Bay Fm. (sandstone, conglomerate) (Figs. 2, 7A). We have included all lithologies present in the geological map (Fig. 2, Mlčoch et al. (2020)), including soils and drift, in our analysis. The coverage of each lithology changes within the sub-catchments, generally with igneous units becoming less important and sedimentary units becoming more important with distance downstream (Fig. 7B). The largest downstream changes can be seen in the proportion of each sub-catchment that is composed of the Hidden Lake Fm., notably at 2490 m from the stream source. The most significant correlation between their proportion (Fig. 7B) within a bed material sub-catchment and the first three principal components from the infrared spectra was seen between the Whisky Bay Fm. and PC-2 ($R^2 = 0.639$, $p < 0.001$, Fig. 7A). The largest R^2 value is between Mendel Fm. and PC-1 although its relationship is not statistically significant ($R^2 = 0.999$, $p = 0.083$, Fig. 7A).

Sediment composition changes downstream and this is very clear in PC-2, and to a lesser extent PC-1 of the infrared spectra data (Fig. 7C). There is little downstream change in some of the more minor components of the stream sediments (PC-3). The three elements present in the bed material samples with the most prominent changes in abundance downstream were magnesium, calcium and iron (Mg, Ca, Fe, Fig. 7D), with each having a peak abundance around 1500 m from the stream source. The majority of suspended sediment samples collected were too small to robustly analyse. However, we can compare the composition of bed material samples with the limited number of analysed suspended sediment samples. Whilst the infrared reflectance of bed material and suspended sediment are not identical, there are similar patterns which is also supported by XRF data (supplementary data files SI 5a); notably in the undulation between ~ 350 to 500 nm and 500 to 600 nm, and troughs at ~ 900 nm, 1400 nm, and 1900 nm (Fig. 7E).

In the Algal Stream, possible source material includes Johnson Mesa Fm. breccia, solifluction slope sediments, hyaloclastite breccia, Mendel Fm. (glacigenic, glaciomarine, and marine sediments), St Marta Fm. (sandstone), and Hidden Lake Fm. (claystone, sandstone) (Fig. 8A). The relative proportions of each of these source rocks within each bed material sample sub-catchment are depicted in Fig. 8B. Each has a significant correlation with at least one principal component and, therefore, can be considered as important source rocks, with the most significant correlation, and the largest R^2, being between the St Marta Fm. and PC-2 ($R^2 = 0.848$, $p < 0.001$). However, the downstream trend in the proportions of different lithologies in Algal Stream sub-catchments shows the opposite pattern to that within the Bohemian catchment, with the coverage of igneous rocks increasing downstream and the coverage of sedimentary rocks decreasing. Nevertheless, sedimentary rocks are still the most abundant type of rock in each sub-catchment. Igneous rocks have their largest proportion 1580 m from stream source in Algal Stream (Fig. 8B).

Much like the Bohemian Stream, the composition of bed material changes and is most clearly shown by PC-1 and PC-2 (Fig. 8C). Few elements present in bed material samples showed a clear change downstream for the Algal catchment. Those that did show variability were phosphorus, potassium and silicon (P, K, Si, Fig. 8D). P and Si show a slight increase in abundance with distance downstream, while K has a more sinuous trend, peaking around 1500 m from the stream source. P and Si also appear to have a degree of sinuosity in their downstream composition – in all cases the frequencies of these are between 1500 and 2000 m, suggesting a distinct change in bed material composition every 750 to 1000 m.

Like the Bohemian Stream, there is a distinct similarity between the bed material and infrared spectra, which is also supported by XRF data (supplementary data files SI 5a), following a broad peak at ~ 350 to 500 nm and 500 to 600 nm, and troughs at ~ 1400 nm, and 1900 nm (Fig. 8E). The differences between the Bohemian sediment spectra (Fig. 7E) and Algal sediment spectra (Fig. 8E) should be noted: with the 350 to 500 nm peak being much more variable in the Bohemian catchment's sediments and the Algal sediments lack a trough at ~900 nm.

4. Discussion

4.1. Provenance of bed material

In both catchments, we see that the availability of different rock types changes downstream. This, combined with changes in the chemical and spectral composition of the sediments (Fig. 7C, D; Fig. 8C, D), makes it likely that new sediment is being supplied into the stream, rather than the primary source of sediment is in the uplands of the catchments and sediment composition changing as a consequence of the selective deposition of heavier minerals (Paola et al., 1992), though this likely has an impact on sediment composition as well. This is further supported by the fact that there is a statistically significant relationship between changes in lithology-type and sediment composition (Fig. 7A, Fig. 8A). The highest correlation between the proportional coverage of sub-catchment geology and bed material sample composition was for the geological units that underlie the main river channels (Fig. 2, Fig. 7A, Fig. 8A). In the case of the Bohemian Stream this is the Whisky Bay Fm., while in the Algal Stream, it is the Hidden Lake Fm. and St Marta Fm.. This pattern is also further supported by the geochemistry (XRF) data, where there is a downstream reduction in the proportion of Mg, Ca and Fe occurs in bed material samples from 1500 m from the Bohemian Stream source (Fig. 7C, Fig. 8C). The igneous rocks, including basalt, breccia and tuffs, in the uplands of the Bohemian Stream catchment are enriched in these elements relative to the sedimentary rocks (e.g. Whisky Bay Fm.). This may be due to the high rate of chemical weathering that occurs in the region (Vašinka et al., 2020).

In the Algal catchment, the proportion of bed material sediment composed of P and Si increases with distance downstream. These elements are both far more abundant in igneous rocks (notably hyaloclastite breccias) in the region and suggest these rock units may have some impact on the composition of bed material in the lower reaches of the stream. The downstream increase in the proportion of these elements suggests that, although the sedimentary rocks within the catchment are likely to be the largest contributor of material to the streams, igneous rocks may have more of an impact on the Algal Stream bed material sediments than previously thought (Sroková and Nývlt, 2021). The variability in K, however, is a little less clear. Its initial high level is consistent with the dominance of the St Marta Fm. in the source area of the stream, which is relatively enriched in K. The dip in concentration around 1000 m (Fig. 8C) coincides with an increase in the proportion of igneous rocks in the catchment; indeed some small tributaries come from permafrost-affected soils which overlay breccia, as well as from scree slopes with breccia and basalt clasts, which are relatively depleted in K. The subsequent increase downstream in K is consistent with the understanding that the underlying lithologies (Hidden Lake Fm. and St Marta Fm.) are primary sediment sources. The decrease to a minimum at

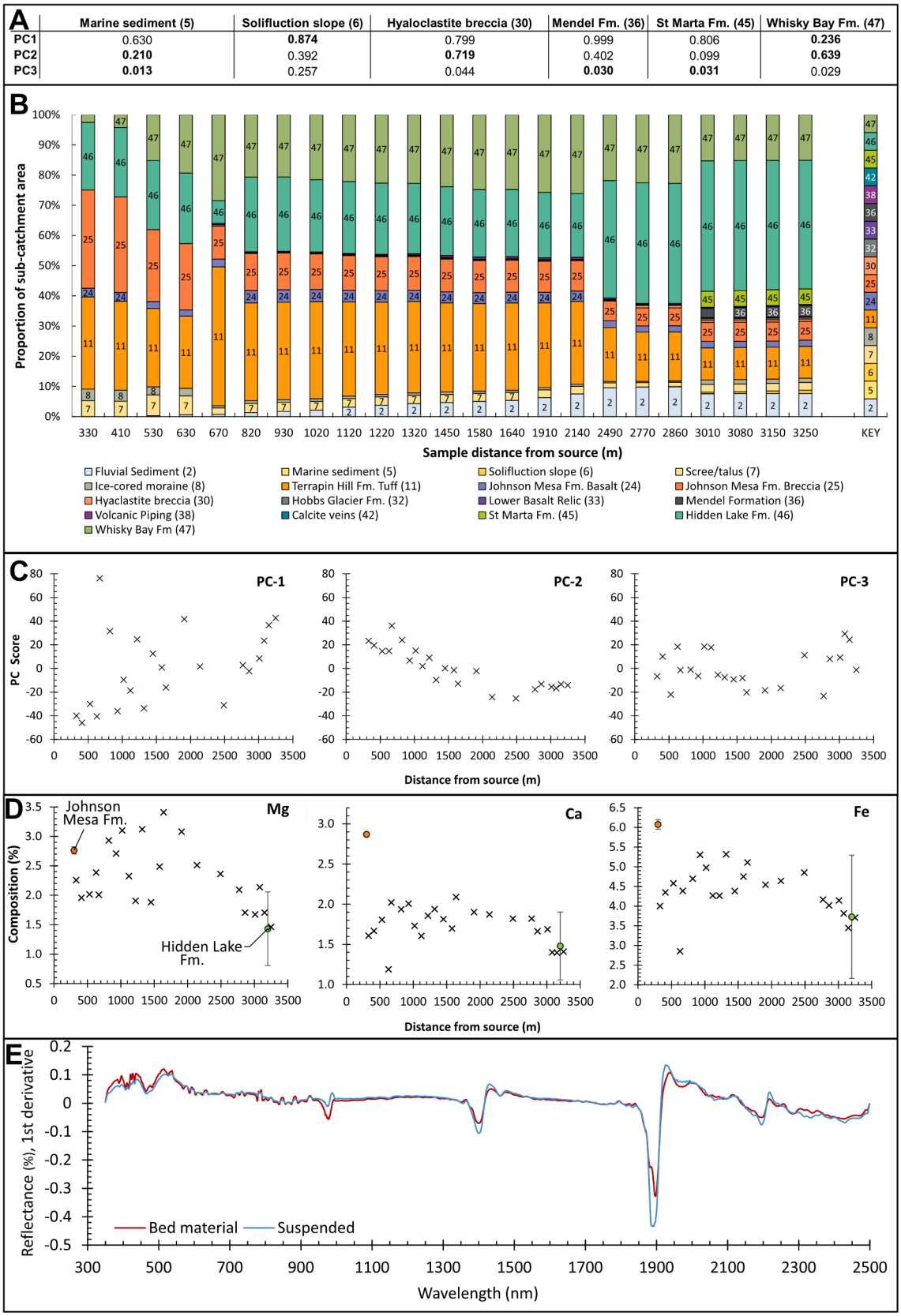

	Marine sediment (5)	Solifluction slope (6)	Hyaloclastite breccia (30)	Mendel Fm. (36)	St Marta Fm. (45)	Whisky Bay Fm. (47)
PC1	0.630	**0.874**	0.799	0.999	0.806	**0.236**
PC2	**0.210**	0.392	**0.719**	0.402	0.099	**0.639**
PC3	**0.013**	0.257	0.044	**0.030**	**0.031**	0.029

Fig. 7. The geochemical variation in the sediments of the Bohemian Stream. **A)** shows the R^2 value between the proportion of the sub-catchment of major lithologies and the principal component score of those samples, bold values indicate a significant correlative relations ($p < 0.05$); **B)** shows the downstream changes in the proportion of rock-types within the subcatchment of each bed material sample, NB: the X axis is not continuous; **C)** shows the downstream changes in principal component scores; **D)** shows the downstream changes in magnesium, calcium and iron, and the % of these elements within the largest lithological unit at . source and at the furthest downstream point; **E)** shows the mean first derivative reflected of bed material and suspended sediments (from across the Bohemian catchment, n = 10)

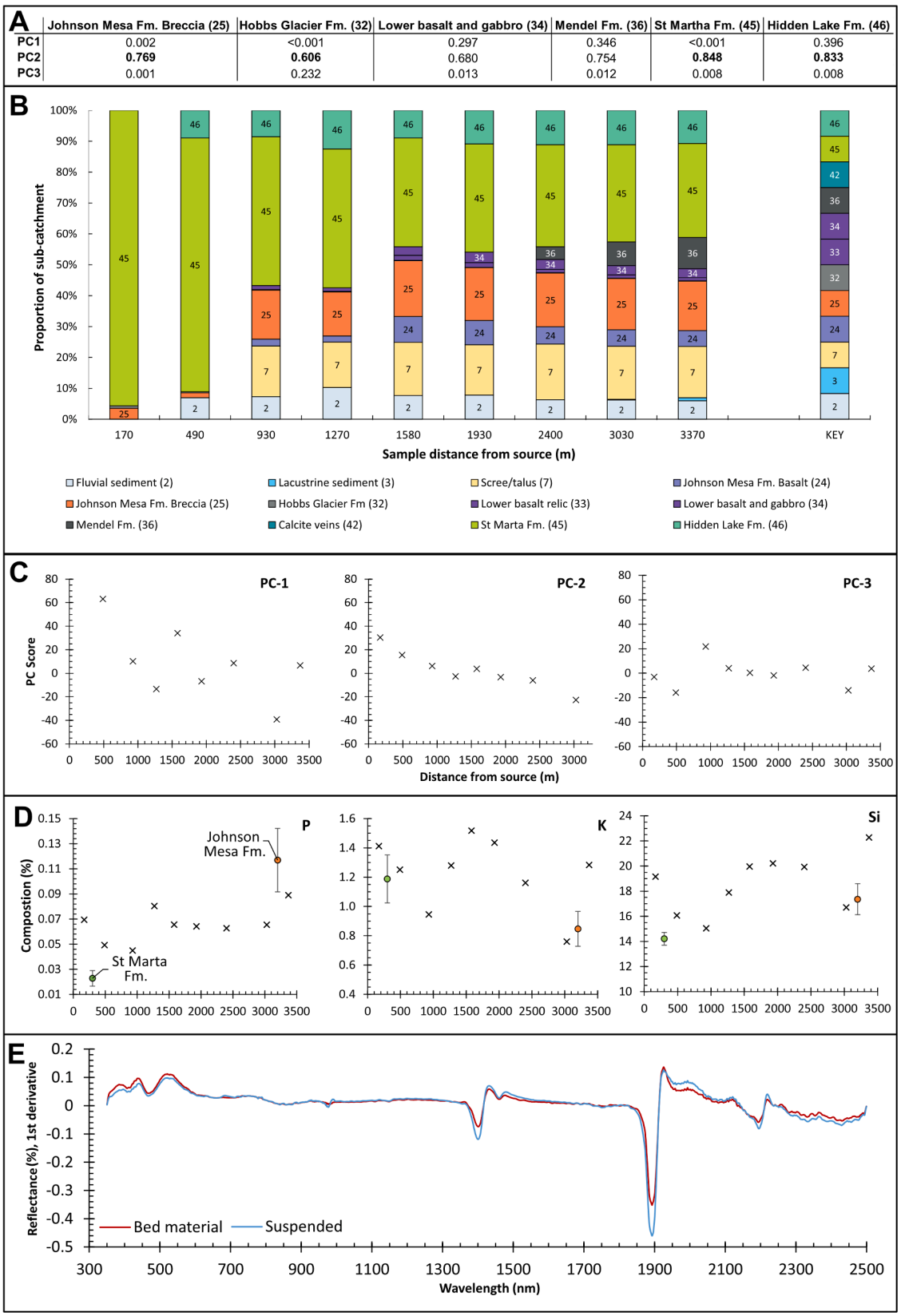

Fig. 8. The geochemical variation in the sediments of the Algal Stream. **A)** shows the R^2 value between the proportion of the sub-catchment of major lithologies and the principal component score of those samples, bold values indicate a significant correlative relations ($p < 0.05$); **B)** shows the downstream changes in the proportion of rock-types within the sub-catchment of each bed material sample, NB: the X axis is not continuous; **C)** shows the downstream changes in principal component scores; **D)** shows the downstream changes in Phosphorus, Potassium and Silicon, and the % of these elements within the largest lithological unit at . source and the second largest at the furthest downstream point; **E)** shows the mean first derivative reflected of bed material and suspended sediments, n = 5

3000 m (Fig. 8C) from the Algal Stream source could be explained by the stream flowing over the Mendel Fm., which has slightly lower recorded K values than the Hidden Lake Fm. and St Marta Fm. The final spike in K (Fig. 8C) is possibly due to the stream cutting into Holocene marine sediments. The influence of the Mendel Fm. may also account for some of the apparent importance of volcanic material in the lower reach of the Algal Stream. The Mendel Fm. is mostly glacigenic to glaciomarine in origin and is composed of clasts from the James Ross Island Volcanic Group, including Johnson Mesa Fm. breccia and basalt (Nývlt et al., 2011). Given the Algal Stream cuts through the Mendel Fm. in its lower reaches, this is a likely source of the igneous influence on Algal Stream sediments; indeed the Algal stream does erode down significantly, as it flows over this unit. Another possible source of sediment is the ice cave above the Algal Stream (Fig. 10B-1, supplementary document SI 1a), which is covered by fine aeolian and slope sediment and is likely to also increase sediment export on days with positive air temperatures.

For both of these catchments, the dominance of underlying strata on the composition of the streams suggests that transport capacity for bed material is low; i.e. that the transport regime is transport-limited (at least in the < 2 mm sediment fraction), and that transport distances are short (likely < 1 km), an interpretation that is consistent with the low discharge values measured in these streams and is supported by previous work in the region (Sroková and Nývlt, 2021). However, we are confident that the bed material < 2 mm in size is mobile in these streams, with little armouring present, and we observed some transportation by traction and saltation (see supplementary video).

Whilst the small sample sizes of suspended sediment mean an in-depth analysis of their provenance is challenging, the similarity in the spectra with bed material suggests that their sources are likely to be similar. This is also supported by the fact that the composition of suspended sediment samples varies with discharge, albeit with only a small number of data points (Fig. 9). Indeed, this interpretation is statistically supported and there is a correlation between PC-1 of the IRS data and discharge; suggesting sediment composition is controlled by discharge; likely due to the transport distance of sediment entrained from the braidplain increasing with higher discharge. At BL ($r = -1.00$, $p = 0.08$, $n = 4$), and at AL ($r = -0.50$, $p = 0.66$, $n = 3$) we see a strong negative correlation (Spearman's rank), which supports interpretations made in previous studies that the braidplain is an important source of suspended sediment material (Kavan et al., 2017). Additionally, given the amount of sediment the Dirty Stream deposits onto the braidplain (Fig. 9A), it also supports research suggesting the importance of the Dirty Stream as a key source of sediment exported from the Bohemian Stream (Sroková and Nývlt, 2021).

Sediment from outside of the catchment itself may also be an input to these streams via wind transportation (Kavan et al., 2017). Aeolian activity is especially high at the end of the summer season when the surface is dry and a large amount of material is available for entrainment and transport (Kavan et al., 2018). Most of the material is transported a short distance. However, the deposition of long-range transported material has been identified on local glaciers (Kavan et al., 2020). Preliminary analysis (Kavan and Nývlt, 2018) suggests that the braidplain and riparian zones of the Bohemian Stream act as a temporary deposition centre for fine-grained aeolian material, which is later activated and transported when the stream is flowing with a high discharge. The prevailing winds favour the transport of iron-rich material originating from the volcanic rocks of Johnson Mesa to the study catchment. This may have an impact on the geochemistry of fluvial samples and may account for the small input of volcanic sediments in the streams.. The interaction of fluvial and aeolian processes has been observed in several Arctic sites (Bachelder et al., 2020; Bullard and Austin, 2011; Crusius et al., 2011; Good and Bryant, 1985), although most of the studies consider the braidplain with its fluvial sediments as a source for further aeolian transport, rather than aeolian material providing sediment to the river network.

4.2. *Suspended sediment transport and variability*

4.2.1. *Suspended sediment transport*

The Algal Upper site typically has a lower specific sediment load than the Algal Lower site (Fig. 6). This suggests new sediment is entrained in the lowermost part of the river, perhaps due to changes in stream gradient and the unlithified material of the Mendel Fm., which are then deposited on a small delta. The upper Algal stream is rather flat, with the lower stream cutting through the strata, making a steeper valley (see supplementary document SI 1b) and sediment being supplied from permafrost-affected soils, slopes, and snowpacks in the lower reaches of the stream. This is consistent with the large sediment deposits in the upper parts of the Algal catchment (Fig. 10B-2).

In the Bohemian catchment, we found the Bohemian Upper site only flowed if there had been recent warm temperatures causing snowmelt on Johnson Mesa and the surrounding uplands. However, when the water did flow, we found this site had significantly higher sediment loads than the Bohemian Lower site (Fig. 5), which is surprising given its small area

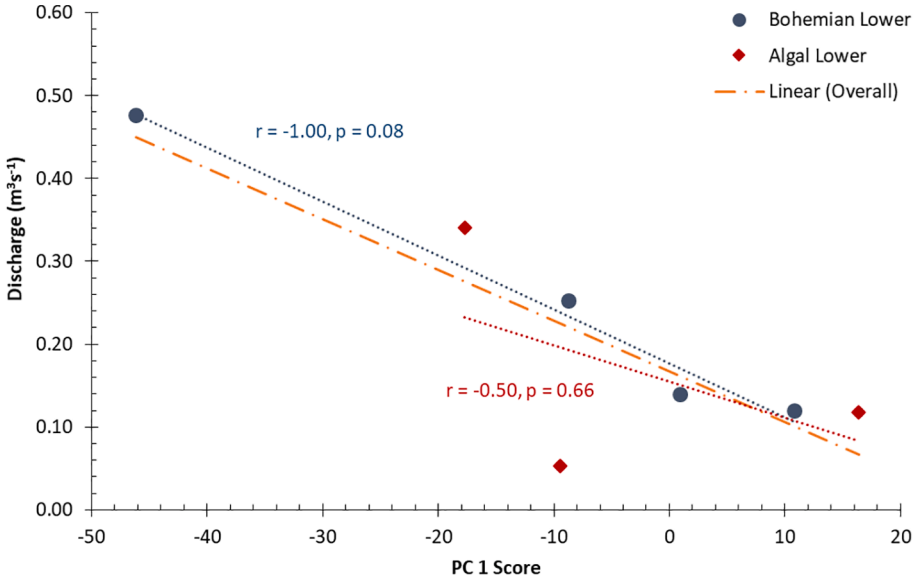

Fig. 9. Relationship between discharge and suspended sediment concentration, as described by PC-1 of infrared spectra.

and suggests there is substantial deposition in the middle section of the Bohemian catchment; consistent with field observations. The same can be said for the Dirty Stream (a major tributary), whose specific sediment loads are larger than that of the Bohemian Lower due to its higher gradient. Furthermore, large alluvial fans at the confluence of the Dirty Stream and Bohemian Stream and upstream (Fig. 10A-2) evidence pronounced deposition to the Bohemian Stream's braidplain from several tributaries from the southeast. This interpretation is consistent with the negative relationship observed between precipitation and discharge (Figs. 4,5) in both catchments. This relationship is likely because the primary form of precipitation is snowfall, and there is typically a lag time of several days between peak snowfall and peak discharge as this snow melts, as well as precipitation typically coinciding with lower air temperature.

4.2.2. A conceptual model of the drivers of suspended sediment variability

Data from both continuous measurement sites (Fig. 4,5) show that high precipitation followed by high temperatures is associated with higher rates of melt of snowfields, ice, and the active layer, and is a key control on suspended sediment concentration and, therefore, sediment load. The sediment load of both catchments is therefore highly sensitive to changes in water availability and suggests that both of the river catchments are broadly transport-limited. This interpretation is consistent with the geomorphology; the presence of large sediment sinks (Fig. 10), including braidplains and fans, and the high availability of unconsolidated sediments owing to it having previously been heavily glacierised (Davies et al., 2013; Jennings et al., 2021). Additionally, the local Cretaceous sedimentary rocks of this region are very friable (Ineson et al., 1986) and they remain largely unconsolidated due to James Ross Island's semi-arid climate preventing the growth of vegetation (Nývlt et al., 2016). A transport-limited regime is further suggested by the exceptionally large specific sediment load value (1984 kg/min/km^2, Fig. 5) measured at the Bohemian Upper site on 22 January. During this time, there was a brief but rapid snowmelt that increased the risk of slope failure (Decaulne et al., 2005; Kňažková et al., 2021), which we observed in the field (see supplementary document, SI 2a), manifesting in a large volume of unconsolidated sediments becoming available to the stream. These episodes of short-lived but very high sediment loads suggest: **i)** the sediment delivery ratio during these events was high, which is intuitive given the high slope angles of the sites and the rapid meltwater production at the time (Wan et al., 2019), and; **ii)** the fluvial energy is not sustained downstream, likely due to changes in stream gradient, and so the deposition rate was high because this very high sediment load value did not occur at the Bohemian Lower site (Fig. 5). This interpretation is reinforced by field observations showing a substantial volume of deposited sediment around the Bohemian Upper site (see supplementary document, SI 2b). Whilst broadly transport-limited, the supply of additional aeolian sediment over the winter period to the braidplain of both streams likely results in additional sediment being available for transport, and is probably why sediment loads in the earlier parts of the summer season are higher despite similar hydrological conditions (Figs. 4b, 5b, 6).

Furthermore, this interpretation is consistent with the measured "flash flood" event experienced on the Bohemian catchment between 17

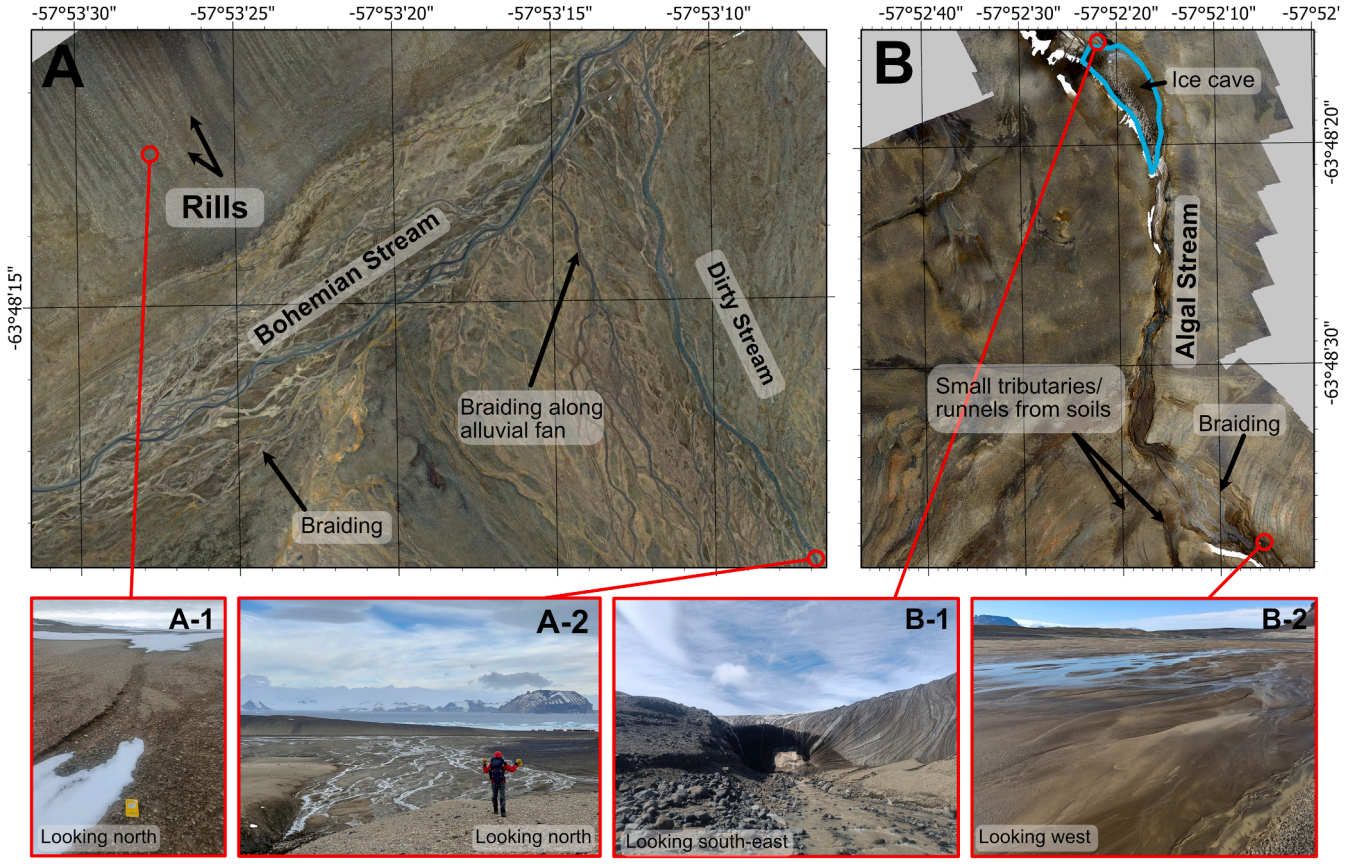

Fig. 10. UAV images of: **A)** the confluence between the Bohemian Stream (main channel) and Dirty Stream and; **B**) the Algal Stream, with its ice cave and braiding highlighted. Note in both catchments the large areas of unconsolidated sediments on the braidplains of all three streams. **A-1** shows rilling near the Bohemian Stream (notebook for scale), **A-2** shows the confluence of the Dirty Stream with the Bohemian Stream. **B-1** shows the ice cave front on the Algal Stream, while **B-2** shows unconsolidated sediment on an Algal Stream braidplain. Both main images were taken by MK using a DJI Mavic 2 Pro UAV. Inset photos were taken by CS, except A-2, which was taken by Lucie Ráčková.

and 19 February (Fig. 4) and between 16 and 23 January in the Algal Stream (Fig. 5). These kinds of rapid sediment transport events are consistent with previous work in this region (Kavan et al., 2017), which states that much of the seasonal sediment delivery happens over the course of a small number of flood events and is represented in our discharge data (Fig. 4, Fig. 5). Indeed, work in other cold regions has highlighted that a significant proportion of the sediment delivery of streams in sub-polar and alpine catchments occurs during short-duration flood events (e.g. Lenzi et al., 2003; Orwin and Smart, 2004; Willems et al., 2011; Yde et al., 2014; Eagle et al., 2021). It is of note that flash flood events appear to follow snowfall events, but not rainfall events (Figs. 4, 5). This likely represents a difference in ground conditions in the upper parts of the catchment. Frozen ground is less porous and, as snowmelts in upland regions, infiltration rates are low and water is channelled more efficiently into the streams (Coles and McDonnell, 2018). In contrast, the rainfall events occurred after a period of sustained > 0 °C, when infiltration rates in the uplands are likely to be higher. Whereas peaks in sediment load are associated with rising air temperatures in the Bohemian catchment, the drivers of sediment load variability are more complicated in the Algal catchment. Although the peak at the end of the season appears to be associated with rising air temperatures following a snowfall event, the earlier peak follows an increase in active layer thaw rate (coincident with a rise in air temperature) on 18 January. Similarly, the high sediment load on 8–9 January for the Algal catchment sites (Fig. 6) coincides with an increase in thaw rate, which rose from -7.8 cmd^{-1} on 6 January to 16.8 cmd^{-1} and 9.8 cmd^{-1} on 7 and 8 January respectively (supplementary data set SI 3). However, due to a fault with the discharge monitor, we do not have continuous data from the stream at that point of the season. Both catchments had relatively short periods of sediment delivery (lasting 3–5 days), with some peaks in SSC being even shorter (e.g. preceding the 19/2 peak in the Bohemian Stream, Fig. 4B). It is also of note that the suspended sediment load from the totally deglaciated Algal catchment is greater than the Bohemian catchment, and indeed both catchments show order of magnitude larger sediment loads compared to other catchments in Antarctica (Inbar, 1995; Mosley, 1988; Chinn and Mason, 2016; Stott and Convey, 2021). This is perhaps because our studied catchments have particularly fissile sediments (Davies et al., 2013). This highlights that even deglaciated catchments can be important sources of sediment to the Southern Ocean.

Overall, variability in SSC from the Bohemian catchment appears to be sensitive to changes in air temperature and precipitation, whilst sediment load from the Algal catchment appears to be more complicated, and shows sensitivity to active layer thaw as well as air temperature/precipitation. However, given the relatively high uncertainties in our measurements, this interpretation cannot be made with high confidence, and further research should aim to investigate this matter more closely.

A possible explanation for these differences between the catchments could be found in the presence of ice masses across the catchments. The Bohemian catchment is home to two small unnamed glaciers on the eastern slopes of Johnson Mesa, which are sometimes unofficially referred to as Crame Col Glacier, at the source of the Dirty Stream, and Johnson Mesa Lakes Glacier, above the Bohemian Upper site at the source of the Bohemian Stream. Glaciers and snowfields are sensitive to air temperature (Engel et al., 2023, 2018), and would be expected to be an important water source (Huss and Hock, 2018; Kavan, 2021). In contrast, no glaciers presently cover the Algal catchment, and its only permanent ice is in the form of a small ice cave (Fig. 10B) just upstream from the Algal Lower site.

Whilst both catchments do respond to precipitation, the magnitude of the response appears far greater in the Bohemian catchment than it is in the Algal catchment, with the most notable response in the Algal catchment being on 19 to 20 February. There is also a difference in drivers of variability at different temporal scales. The sediment load of all five sites can be seen to broadly follow changes in air temperature (Fig. 6) throughout the day, but the magnitude of values on different days varies. We propose that these magnitudes are dependent on different environmental factors in the different catchments and can be considered in the form of a conceptual model (Fig. 11). The Bohemian catchment is sensitive to changes in air temperature, which is intuitive given the presence of glaciers in this catchment. Whereas the Algal catchment, with an absence of ice masses, is more dependent on changes in active layer thickness, though changes in air temperature do affect discharge to some degree (Fig. 5); and indeed air temperature itself controls active layer thaw (Hrbáček et al., 2023). Other studies (e.g. Kavan et al., 2017) have suggested that the Bohemian catchment is also likely to have water sourced from permafrost-affected soils. Although our data do not provide a direct agreement with this, we did observe some small-scale rills on the northern slopes of the Bohemian catchment (Fig. 10 A-1) and permafrost-affected soils are likely a small source of water and, therefore, sediment load variability in the Bohemian Stream. Indeed, the discharge of some Arctic streams are influenced by active layer thaw and permafrost degradation (Karlsson et al., 2015; Song et al., 2020; Wang et al., 2021). Whilst this conceptual model largely confirms what is already known about Alpine and Arctic catchments (Schaefli et al., 2005; Blaen et al., 2014; Carrivick et al., 2018; Carrivick and Tweed, 2021) the spatio-temporal variability in driving mechanisms has not been unravelled for Antarctic catchments. The differences in the way two neighbouring catchments operate partly due to differences in the glacier ice cover is also particularly interesting in the context of melting glaciers and the expansion of proglacial areas in Antarctica (Lee et al., 2017; Engel et al., 2023).

5. Summary and conclusions

Here we have presented an in-depth analysis of river water discharge and sediment transport in two neighbouring catchments on Ulu Peninsula, James Ross Island. We employed stream monitoring and provenance analysis, which are very rare and untried before in Antarctica, respectively, to unravel the spatio-temporal characteristics and drivers of sediment transport controls. Our data show that sediment load from the Bohemian catchment is controlled by air temperature. In contrast, sediment load in the Algal catchment appears to be sensitive to large changes in active layer thickness, as well as to air temperature and precipitation. Exceptionally high suspended sediment loads in the upper reaches of the Bohemian Stream highlight the fact that the streams in this region are sediment transport-limited and that: **i)** there is the potential for the Bohemian Stream to carry large quantities of sediment if there is sufficient water supplied to the channel, and; **ii)** the availability of this water is very sensitive to air temperature, which can result in load differences of five orders of magnitude within 24 h. The sediment loads from these streams are exceptionally high for Antarctica and we estimate that the annual sediment load for the Bohemian Stream in the austral summer of 2021/2022 was 1.18 ± 0.63 t km^{-2} d^{-1} and 1.73 ± 1.02 t km^{-2} d^{-1} yr^{-1} for the Algal Stream.

Bed material in both the Bohemian Stream and Algal Stream is related to the rocks they overlay, notably sedimentary strata due to the very short (<1 km) transport distance of bedload in these rivers. However, minor components of the bed material in both streams are sourced from igneous rocks; in the Bohemian Stream, this is evident in the samples closest to the source, whereas in the Algal Stream, the importance of igneous rocks increases downstream. This is perhaps because permafrost-affected soils overlay units of hyaloclastite breccia, or due to the presence of igneous clasts within the Mendel Fm.

The Bohemian and Algal Streams give a glimpse of the future for many Antarctic catchments as glaciers retreat. The deglaciation of the catchments on James Ross Island has made a large volume of unconsolidated sediment available for transport and, even in the absence of glacial melt, large quantities of this sediment can be transported on days with positive temperatures (which are expected to become more frequent) when the active layer, snow and any other bodies of ice melt.

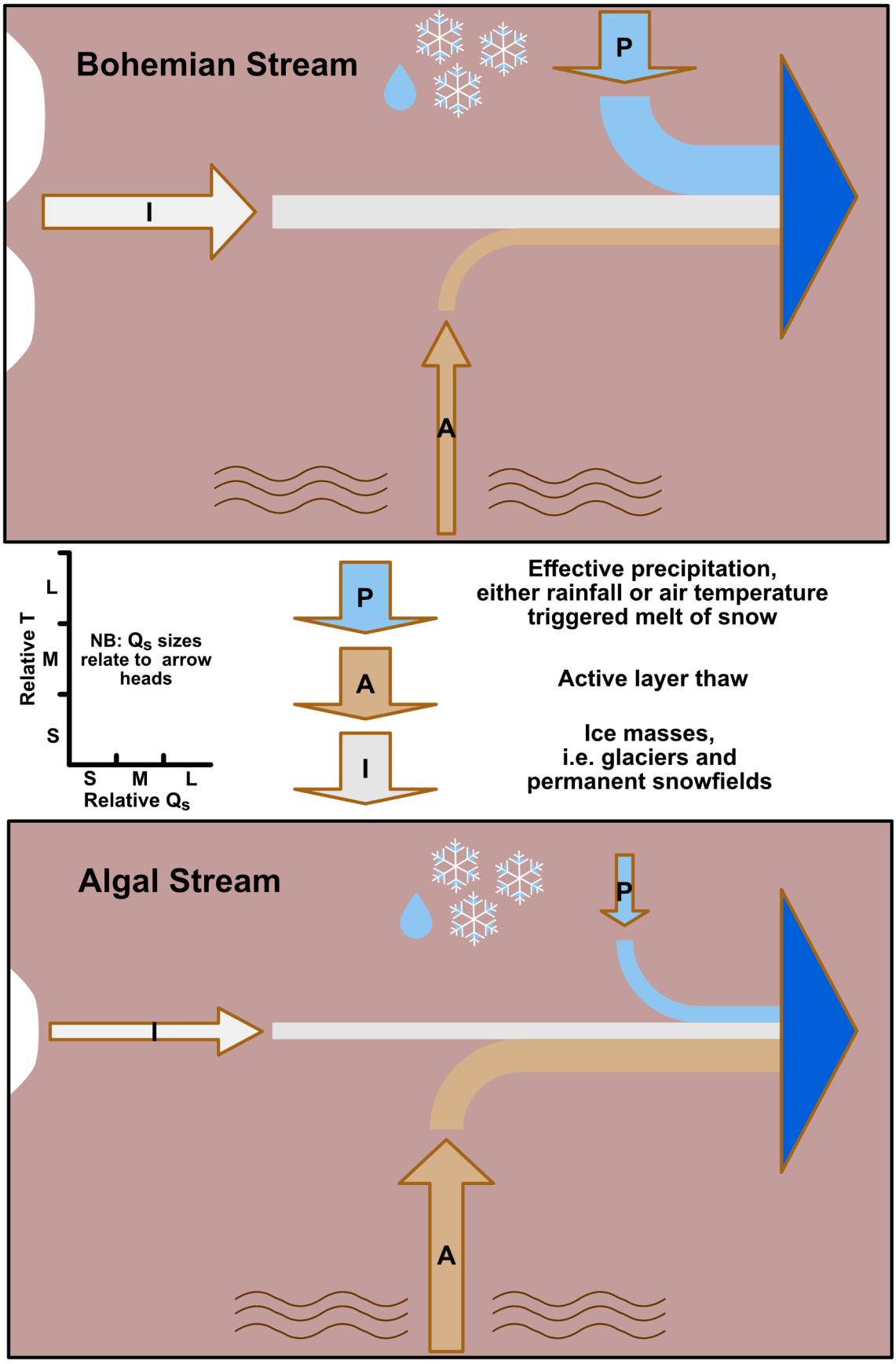

Fig. 11. A conceptual model of the drivers of sediment load variability in both catchments. NB: the ice mass arrows are oriented 90 degrees to the scale. S,M,L = small, medium, large. T = Time, Qs = sediment discharge.

CRediT authorship contribution statement

Christopher D. Stringer: Writing – original draft, Methodology, Funding acquisition, Data curation, Conceptualization. **John F. Boyle:** Methodology, Formal analysis. **Filip Hrbáček:** Methodology, Formal analysis, Data curation. **Kamil Láska:** Funding acquisition, Methodology, Formal analysis. **Ondřej Nedělčev:** Data curation. **Jan Kavan:** Writing – original draft, Formal analysis. **Michaela Kňažková:** Investigation, Writing – review & editing. **Jonathan L. Carrivick:** Supervision, Writing – review & editing. **Duncan J. Quincey:** Supervision, Writing – review & editing. **Daniel Nývlt:** Supervision, Writing – review & editing.

Declaration of competing interest

The authors declare that they have no known competing financial interests or personal relationships that could have appeared to influence the work reported in this paper.

Data availability

To be made available in the supplementary material

Acknowledgements

The Czech Antarctic Research Programme (CARP) are thanked for their support of this project, particularly in accommodating CDS at the Johann Gregor Mendel Czech Antarctic Station on James Ross Island during the austral summer of 2021/22. We also thank all of the staff at CARP for their logistical support. We also gratefully acknowledge the loan of a Spectral Evolution PSR + 3500 spectrometer from the Natural Environment Research Council (NERC) Field Spectroscopy Facility that allowed us to carry out this research, specifically; we would like to thank Andrew Gray of the University of Edinburgh for training CDS on the equipment.

This work is supported by the Leeds-York-Hull NERC Doctoral Training Partnership (DTP) Panorama under grant NE/S007458/1. The Ministry of Education, Youth and Sports of the Czech Republic projects VAN 1/2022 and VAN 1/2023 and the Czech Antarctic Foundation funded fieldwork that contributed to this work. The Czech Science Foundation (project GC20-20240S) funded the meteorological work involved in this study.

Appendix A. Supplementary data

Supplementary data to this article can be found online at https://doi.org/10.1016/j.jhydrol.2024.131157.

References

Ambrozova, K., Laska, K., Hrbacek, F., Kavan, J., Ondruch, J., 2019. Air temperature and lapse rate variation in the ice-free and glaciated areas of northern James Ross Island, Antarctic Peninsula, during 2013–2016. Int. J. Climatol. 39, 643–657. https://doi.org/10.1002/joc.5832.

Bachelder, J., Cadieux, M., Liu-Kang, C., Lambert, P., Filoche, A., Galhardi, J.A., Hadioui, M., Chaput, A., Bastien-Thibault, M.-P., Wilkinson, K.J., King, J., Hayes, P. L., 2020. Chemical and microphysical properties of wind-blown dust near an actively retreating glacier in Yukon, Canada. Aerosol Sci. Technol. 54, 2–20. https://doi.org/10.1080/02786826.2019.1676394.

Ballantyne, C.K., 2008. After the Ice: Holocene Geomorphic Activity in the Scottish Highlands. Scottish Geogr. J. 124, 8–52. https://doi.org/10.1080/14702540802300167.

Bentley, M.J., Hodgson, D.A., Smith, J.A., Cofaigh, C., Domack, E.W., Larter, R.D., Roberts, S.J., Brachfeld, S., Leventer, A., Hjort, C., Hillenbrand, C.-D., Evans, J., 2009. Mechanisms of Holocene palaeoenvironmental change in the Antarctic Peninsula region. The Holocene 19, 51–69. https://doi.org/10.1177/0959683608096603.

Blaen, P.J., Hannah, D.M., Brown, L.E., Milner, A.M., 2014. Water source dynamics of high Arctic river basins. Hydrol. Process. 28, 3521–3538. https://doi.org/10.1002/hyp.9891.

Bullard, J., Austin, M., 2011. Dust generation on a proglacial floodplain. West Greenland. Aeolian Res. 3 https://doi.org/10.1016/j.aeolia.2011.01.002.

Carrasco, J.F., Bozkurt, D., Cordero, R.R., 2021. A review of the observed air temperature in the Antarctic Peninsula. Did the warming trend come back after the early 21st hiatus? Polar Sci. 28, 100653 https://doi.org/10.1016/j.polar.2021.100653.

Carrivick, J.L., Davies, B.J., Glasser, N.F., Nývlt, D., Hambrey, M.J., 2012. Late-Holocene changes in character and behaviour of land-terminating glaciers on James Ross Island. Antarctica. J. Glaciol. 58, 1176–1190. https://doi.org/10.3189/2012JoG11J148.

Carrivick, J.L., Heckmann, T., Turner, A., Fischer, M., 2018. An assessment of landform composition and functioning with the first proglacial systems dataset of the central European Alps. Geomorphology 321, 117–128. https://doi.org/10.1016/j.geomorph.2018.08.030.

Carrivick, J.L., Tweed, F.S., 2021. Deglaciation controls on sediment yield: Towards capturing spatio-temporal variability. Earth-Science Rev. 221, 103809 https://doi.org/10.1016/j.earscirev.2021.103809.

Chinn, T., Mason, P., 2016. The first 25 years of the hydrology of the Onyx River, Wright Valley, Dry Valleys. Antarctica. Polar Rec. (gr. Brit). 52, 16–65. https://doi.org/10.1017/S0032247415000212.

Cloern, J.E., 1987. Turbidity as a control on phytoplankton biomass and productivity in estuaries. Cont. Shelf Res. 7, 1367–1381. https://doi.org/10.1016/0278-4343(87)90042-2.

Coles, A.E., McDonnell, J.J., 2018. Fill and spill drives runoff connectivity over frozen ground. J. Hydrol. 558, 115–128. https://doi.org/10.1016/j.jhydrol.2018.01.016.

Collins, A.L., Blackwell, M., Boeckx, P., Chivers, C.A., Emelko, M., Evrard, O., Foster, I., Gellis, A., Gholami, H., Granger, S., Harris, P., Horowitz, A.J., Laceby, J.P., Martinez-Carreras, N., Minella, J., Mol, L., Nosrati, K., Pulley, S., Silins, U., da Silva, Y.J., Stone, M., Tiecher, T., Upadhayay, H.R., Zhang, Y., 2020. Sediment source fingerprinting: benchmarking recent outputs, remaining challenges and emerging themes. J. Soils Sediments 20, 4160–4193. https://doi.org/10.1007/s11368-020-02755-4.

Cook, A.J., Holland, P.R., Meredith, M.P., Murray, T., Luckman, A., Vaughan, D.G., 2016. Ocean forcing of glacier retreat in the western Antarctic Peninsula. Science (80-.). 353, 283–286. https://doi.org/10.1126/science.aae0017.

Costa, A., Molnar, P., Stutenbecker, L., Bakker, M., Silva, T.A., Schlunegger, F., Lane, S. N., Loizeau, J.-L., Girardclos, S., 2018. Temperature signal in suspended sediment export from an Alpine catchment. Hydrol. Earth Syst. Sci. 22, 509–528. https://doi.org/10.5194/hess-22-509-2018.

Crusius, J., Schroth, A.W., Gassó, S., Moy, C.M., Levy, R.C., Gatica, M., 2011. Glacial flour dust storms in the Gulf of Alaska: Hydrologic and meteorological controls and their importance as a source of bioavailable iron. Geophys. Res. Lett. 38.

Czech Geological Survey, 2009. Map of Northern Part of James. Ross Island.

Davies, B.J., Glasser, N.F., Carrivick, J.L., Hambrey, M.J., Smellie, J.L., Nývlt, D., 2013. Landscape evolution and ice-sheet behaviour in a semi-arid polar environment: James Ross Island, NE Antarctic Peninsula. Geol. Soc. London. Spec. Publ. 381, 353–395. https://doi.org/10.1144/SP381.1.

Decaulne, A., Sæmundsson, P., Pétursson, O., 2005. Debris flow triggered by rapid snowmelt: A case study in the Gleidarhjalli area, northwestern Iceland. Geogr. Ann. Ser. A Phys. Geogr. 87, 487–500. https://doi.org/10.1111/j.0435-3676.2005.00273.x.

Eagle, L.J.B., Carrivick, J.L., Milner, A.M., Brown, L.E., Klaar, M.J., 2021. Repeated high flows drive morphological change in rivers in recently deglaciated catchments. Earth Surf. Process. Landforms 46, 1294–1310. https://doi.org/10.1002/esp.5098.

Engel, Z., Láska, K., Nývlt, D., Stachoň, Z., 2018. Surface mass balance of small glaciers on James Ross Island, north-eastern Antarctic Peninsula, during 2009–2015. J. Glaciol. 64, 349–361. https://doi.org/10.1017/jog.2018.17.

Engel, Z., Láska, K., Kavan, J., Smolíková, J., 2023. Persistent mass loss of Triangular Glacier, James Ross Island, north-eastern Antarctic Peninsula. J. Glaciol. 69, 27–39. https://doi.org/10.1017/jog.2022.42.

Friedlander, A.M., Goodell, W., Salinas-de-León, P., Ballesteros, E., Berkenpas, E., Capurro, A.P., Cárdenas, C.A., Hüne, M., Lagger, C., Landaeta, M.F., Muñoz, A., Santos, M., Turchik, A., Werner, R., Sala, E., 2020. Spatial patterns of continental shelf faunal community structure along the Western Antarctic Peninsula. PLoS One 15, e0239895. https://doi.org/10.1371/journal.pone.0239895.

García-Rodríguez, F., Piccini, C., Carrizo, D., Sánchez-García, L., Pérez, L., Crisci, C., Oaquim, A.B.J., Evangelista, H., Soutullo, A., Azcune, G., Lüning, S., 2021. Centennial glacier retreat increases sedimentation and eutrophication in Subantarctic periglacial lakes: A study case of Lake Uruguay. Sci. Total Environ. 754, 142066 https://doi.org/10.1016/j.scitotenv.2020.142066.

Gerrish, L., Fretwell, P., Cooper, P., 2020. High resolution vector polygons of the Antarctic coastline (7.2). [WWW Document]. UK Polar Data Centre. Nat. Environ. Res. Counc. UK Res. Innov. https://doi.org/10.5285/065B9ABC-1B5A-4FC6-AA57-9052428AA6CA.

Glasser, N.F., Davies, B.J., Carrivick, J.L., Rodés, A., Hambrey, M.J., Smellie, J.L., Domack, E., 2014. Ice-stream initiation, duration and thinning on James Ross Island, northern Antarctic Peninsula. Quat. Sci. Rev. 86, 78–88. https://doi.org/10.1016/j.quascirev.2013.11.012.

Gonçalves, V.N., de Souza, L.M.D., Lirio, J.M., Coria, S.H., Lopes, F.A.C., Convey, P., Carvalho-Silva, M., de Oliveira, F.S., Câmara, P.E.A.S., Rosa, L.H., 2022. Diversity and ecology of fungal assemblages present in lake sediments at Clearwater Mesa, James Ross Island, Antarctica, assessed using metabarcoding of environmental DNA. Fungal Biol. https://doi.org/10.1016/j.funbio.2022.08.002.

Good, T.R., Bryant, I.D., 1985. Fluvio-Aeolian Sedimentation—An Example from Banks Island, N.W.T., Canada. Geogr. Ann. Ser. A. Phys. Geogr. 67, 33–46. https://doi.org/10.1080/04353676.1985.11880128.

Hodson, A., Nowak, A., Sabacka, M., Jungblut, A., Navarro, F., Pearce, D., Ávila-Jiménez, M.L., Convey, P., Vieira, G., 2017. Climatically sensitive transfer of iron to maritime Antarctic ecosystems by surface runoff. Nat. Commun. 8, 14499. https://doi.org/10.1038/ncomms14499.

Howat, I.M., Porter, C., Smith, B.E., Noh, M.-J., Morin, P., 2019. The Reference Elevation Model of Antarctica. Cryosph. 13, 665–674. https://doi.org/10.5194/tc-13-665-2019.

Hrbáček, F., Engel, Z., Kňažková, M., Smolíková, J., 2021. Effect of summer snow cover on the active layer thermal regime and thickness on CALM-S JGM site, James Ross Island, eastern Antarctic Peninsula. CATENA 207, 105608. https://doi.org/10.1016/j.catena.2021.105608.

Hrbáček, F., Oliva, M., Hansen, C., Balks, M., O'Neill, T.A., de Pablo, M.A., Ponti, S., Ramos, M., Vieira, G., Abramov, A., Kaplan Pastíriková, L., Guglielmin, M., Goyanes, G., Francelino, M.R., Schaefer, C., Lacelle, D., 2023. Active layer and permafrost thermal regimes in the ice-free areas of Antarctica. Earth-Science Rev. 242, 104458 https://doi.org/10.1016/j.earscirev.2023.104458.

Humlum, O., Instanes, A., Sollid, J.L., 2003. Permafrost in Svalbard: a review of research history, climatic background and engineering challenges. Polar Res. 22, 191–215. https://doi.org/10.1111/j.1751-8369.2003.tb00107.x.

Huss, M., Hock, R., 2018. Global-scale hydrological response to future glacier mass loss. Nat. Clim. Chang. 8, 135–140. https://doi.org/10.1038/s41558-017-0049-x.

Inbar, M., 1995. Fluvial Morphology and Streamflow on Deception Island, Antarctica. Geogr. Ann. Ser. A. Phys. Geogr. 77, 221–230. https://doi.org/10.2307/521331.

Ineson, J.R., Crame, J.A., Thomson, M.R.A., 1986. Lithostratigraphy of the Cretaceous Strata of West James Ross Island. Antarctica. Cretac. Res. 7, 141–159. https://doi.org/10.1016/0195-6671(86)90014-5.

Jennings, S.J.A., Davies, B.J., Nývlt, D., Glasser, N.F., Engel, Z., Hrbáček, F., Carrivick, J. L., Mlčoch, B., Hambrey, M.J., 2021. Geomorphology of Ulu Peninsula, James Ross Island. Antarctica. J. Maps 17, 125–139. https://doi.org/10.1080/17445647.2021.1893232.

Kaplan Pastíriková, L., Hrbáček, F., Uxa, T., Láska, K., 2023. Permafrost table temperature and active layer thickness variability on James Ross Island, Antarctic Peninsula, in 2004–2021. Sci. Total Environ. 161690 https://doi.org/10.1016/j.scitotenv.2023.161690.

Karlsson, J.M., Jaramillo, F., Destouni, G., 2015. Hydro-climatic and lake change patterns in Arctic permafrost and non-permafrost areas. J. Hydrol. 529, 134–145. https://doi.org/10.1016/j.jhydrol.2015.07.005.

Kavan, J., 2021. Fluvial transport in the deglaciated Antarctic catchment – Bohemian Stream, James Ross Island. Geogr. Ann. Ser. a, Phys. Geogr. 1–10. https://doi.org/10.1080/04353676.2021.2010401.

Kavan, J., Nývlt, D., 2018. Where does the Antarctic fluvial suspended sediment come from?

Kavan, J., Ondruch, J., Nývlt, D., Hrbáček, F., Carrivick, J.L., Láska, K., 2017. Seasonal hydrological and suspended sediment transport dynamics in proglacial streams, James Ross Island, Antarctica. Geogr. Ann. Ser. A. Phys. Geogr. 99, 38–55. https://doi.org/10.1080/04353676.2016.1257914.

Kavan, J., Dagsson-Waldhauserova, P., Renard, J.B., Láska, K., Ambrožová, K., 2018. Aerosol concentrations in relationship to local atmospheric conditions on James Ross Island, Antarctica. Front. Earth Sci. 0–0 https://doi.org/10.3389/feart.2018.00207.

Kavan, J., Nývlt, D., Láska, K., Engel, Z., Kňažková, M., 2020. High-latitude dust deposition in snow on the glaciers of James Ross Island, Antarctica. Earth Surf. Process. Landforms 45, 1569–1578. https://doi.org/10.1002/esp.4831.

Kavan, J., Hrbáček, F., Stringer, C.D., 2023. Proglacial streams runoff dynamics in Devíls Bay, Vega Island, Antarctica. Hydrol. Sci. J. 1–15 https://doi.org/10.1080/02626667.2023.2195559.

Kňažková, M., Nývlt, D., Hrbáček, F., 2021. Slope processes connected with snow patches in semi-arid ice-free areas of James Ross Island, Antarctic Peninsula. Geomorphology 373, 107479. https://doi.org/10.1016/j.geomorph.2020.107479.

Košler, J., Magna, T., Mlčoch, B., Mixa, P., Nývlt, D., Holub, F.V., 2009. Combined Sr, Nd, Pb and Li isotope geochemistry of alkaline lavas from northern James Ross Island (Antarctic Peninsula) and implications for back-arc magma formation. Chem. Geol. 258, 207–218. https://doi.org/10.1016/j.chemgeo.2008.10.006.

Lee, J.R., Raymond, B., Bracegirdle, T.J., Chadès, I., Fuller, R.A., Shaw, J.D., Terauds, A., 2017. Climate change drives expansion of Antarctic ice-free habitat. Nature 547, 49–54. https://doi.org/10.1038/nature22996.

Lenzi, M.A., Mao, L., Comiti, F., 2003. Interannual variation of suspended sediment load and sediment yield in an alpine catchment. Hydrol. Sci. J. 48, 899–915. https://doi.org/10.1623/hysj.48.6.899.51425.

Łepkowska, E., Stachnik, Ł., 2018. Which Drivers Control the Suspended Sediment Flux in a High Arctic Glacierized Basin (Werenskioldbreen, Spitsbergen)? Water 10, 1408. https://doi.org/10.3390/w10101408.

Lipp, A.G., Roberts, G.G., Whittaker, A.C., Gowing, C.J.B., Fernandes, V.M., 2021. Source Region Geochemistry From Unmixing Downstream Sedimentary Elemental Compositions. Geochemistry, Geophys. Geosystems 22, e2021GC009838. https://doi.org/10.1029/2021GC009838.

Mlčoch, B., Nývlt, D., Mixa, P., 2020. Geological map of James Ross Island-Northern part 1: 25,000. Czech Geological Survey, Praha.

Mosley, M., 1988. Bedload transport and sediment yield in the Onyx River, Antarctica. Earth Surf. Process. Landforms 13, 51–67. https://doi.org/10.1002/esp.3290130108.

Mulvaney, R., Abram, N.J., Hindmarsh, R.C.A., Arrowsmith, C., Fleet, L., Triest, J., Sime, L.C., Alemany, O., Foord, S., 2012. Recent Antarctic Peninsula warming relative to Holocene climate and ice-shelf history. Nature 489, 141–144. https://doi.org/10.1038/nature11391.

Nehyba, S., Nývlt, D., 2014. Deposits of pyroclastic mass flows at Bibby Hill (Pliocene, James Ross Island, Antarctica). Czech Polar Reports 4, 103–122. https://doi.org/10.5817/CPR2014-2-11.

Nývlt, D., Košler, J., Mlčoch, B., Mixa, P., Lisá, L., Bubík, M., Hendriks, B.W.H., 2011. The Mendel Formation: Evidence for Late Miocene climatic cyclicity at the northern tip of the Antarctic Peninsula. Palaeogeogr. Palaeoclimatol. Palaeoecol. 299, 363–384. https://doi.org/10.1016/j.palaeo.2010.11.017.

Nývlt, D., Braucher, R., Engel, Z., Mlčoch, B., 2014. Timing of the Northern Prince Gustav Ice Stream retreat and the deglaciation of northern James Ross Island, Antarctic Peninsula during the last glacial-interglacial transition. Quat. Res. (united States) 82, 441–449. https://doi.org/10.1016/j.yqres.2014.05.003.

Nývlt, D., Fišáková, M.N., Barták, M., Stachoň, Z., Pavel, V., Mlčoch, B., Láska, K., 2016. Death age, seasonality, taphonomy and colonization of seal carcasses from Ulu Peninsula, James Ross Island, Antarctic Peninsula. Antarct. Sci. 28, 3–16. https://doi.org/10.1017/S095410201500036X.

Oliva, M., Ruiz-Fernández, J., 2015. Coupling patterns between para-glacial and permafrost degradation responses in Antarctica. Earth Surf. Process. Landforms 40, 1227–1238. https://doi.org/10.1002/esp.3716.

Oliva, M., Antoniades, D., Giralt, S., Granados, I., Pla-Rabes, S., Toro, M., Liu, E.J., Sanjurjo, J., Vieira, G., 2016. The Holocene deglaciation of the Byers Peninsula (Livingston Island, Antarctica) based on the dating of lake sedimentary records. Geomorphology 261, 89–102. https://doi.org/10.1016/j.geomorph.2016.02.029.

Orwin, J.F., Smart, C.C., 2004. Short-term spatial and temporal patterns of suspended sediment transfer in proglacial channels, Small River Glacier. Canada. Hydrol. Process. 18, 1521–1542. https://doi.org/10.1002/hyp.1402.

Overeem, I., Hudson, B.D., Syvitski, J.P.M., Mikkelsen, A.B., Hasholt, B., van den Broeke, M.R., Noël, B.P.Y., Morlighem, M., 2017. Substantial export of suspended sediment to the global oceans from glacial erosion in Greenland. Nat. Geosci. 10, 859–863. https://doi.org/10.1038/ngeo3046.

Palerme, C., Genthon, C., Claud, C., Kay, J.E., Wood, N.B., L'Ecuyer, T., 2017. Evaluation of current and projected Antarctic precipitation in CMIP5 models. Clim. Dyn. 48, 225–239. https://doi.org/10.1007/s00382-016-3071-1.

Paola, C., Parker, G., Seal, R., Sinha, S.K., Southard, J.B., Wilcock, P.R., 1992. Downstream Fining by Selective Deposition in a Laboratory Flume. Science (80-.). 258, 1757–1760. https://doi.org/10.1126/science.258.5089.1757.

Russell, F.E., Boyle, J.F., Chiverrell, R.C., 2019. NIRS quantification of lake sediment composition by multiple regression using end-member spectra. J. Paleolimnol. 62, 73–88. https://doi.org/10.1007/s10933-019-00076-2.

Schaefli, B., Hingray, B., Niggli, M., Musy, A., 2005. A conceptual glacio-hydrological model for high mountainous catchments. Hydrol. Earth Syst. Sci. 9, 95–109. https://doi.org/10.5194/hess-9-95-2005.

Shahrestani, S., Mokhtari, A.R., Fatehi, M., 2020. The use of unmixing technique in stream sediment geochemical exploration. J. Geochemical Explor. 208, 106339. https://doi.org/10.1016/j.gexplo.2019.106339.

Smellie, J.L., Johnson, J.S., McIntosh, W.C., Esser, R., Gudmundsson, M.T., Hambrey, M. J., van Wyk de Vries, B., 2008. Six million years of glacial history recorded in volcanic lithofacies of the James Ross Island Volcanic Group, Antarctic Peninsula. Palaeogeogr. Palaeoclimatol. Palaeoecol. 260, 122–148. https://doi.org/10.1016/j.palaeo.2007.08.011.

Song, C., Wang, G., Mao, T., Dai, J., Yang, D., 2020. Linkage between permafrost distribution and river runoff changes across the Arctic and the Tibetan Plateau. Sci. China Earth Sci. 63, 292–302.

Sroková, S., Nývlt, D., 2021. Bedload geochemical and petrophysical signature of the Algal and Bohemian streams, James Ross Island, Antarctic Peninsula. Czech Polar Reports 11, 203–214. https://doi.org/10.5817/CPR2021-2-14.

Staines, K.E.H., Carrivick, J.L., Tweed, F.S., Evans, A.J., Russell, A.J., Jóhannesson, T., Roberts, M., 2015. A multi-dimensional analysis of pro-glacial landscape change at Sólheimajökull, southern Iceland. Earth Surf. Process. Landforms 40, 809–822. https://doi.org/10.1002/esp.3662.

Stott, T., Convey, P., 2021. Seasonal hydrological and suspended sediment transport dynamics and their future modelling in the Orwell Glacier proglacial stream, Signy Island, Antarctica. Antarct. Sci. 33, 192–212. https://doi.org/DOI: 10.1017/S0954102020000607.

Syvitski, J.P.M., 2002. Sediment discharge variability in Arctic rivers: implications for a warmer future. Polar Res. 21, 323–330. https://doi.org/10.3402/polar.v21i2.6494.

Vašinka, M., Krmíček, L., Všianský, D., Hrbáček, F., Nývlt, D., 2020. Chemical weathering in Antarctica: an example of igneous rock particles in Big Lachman Lake sediments. James Ross Island. Environ. Earth Sci. 79, 186. https://doi.org/10.1007/s12665-020-08926-3.

Vaughan, D.G., Marshall, G.J., Connolley, W.M., Parkinson, C., Mulvaney, R., Hodgson, D.A., King, J.C., Pudsey, C.J., Turner, J., 2003. Recent Rapid Regional Climate Warming on the Antarctic Peninsula. Clim. Change 60, 243–274. https://doi.org/10.1023/A:1026021217991.

Wan, D., Li, F., Yu, W., Chen, C., Gao, Y., 2019. Sediment delivery of partially-unfrozen loam soil rill by snow/glacier meltwater flow. Sci. Rep. 9, 3954. https://doi.org/10.1038/s41598-019-40400-4.

Wang, P., Huang, Q., Pozdniakov, S.P., Liu, S., Ma, N., Wang, T., Zhang, Y., Yu, J., Xie, J., Fu, G., Frolova, N.L., Liu, C., 2021. Potential role of permafrost thaw on increasing Siberian river discharge. Environ. Res. Lett. 16, 34046. https://doi.org/10.1088/1748-9326/abe326.

Willems, B.A., Powell, R.D., Cowan, E.A., Jaeger, J.M., 2011. Glacial outburst flood sediments within Disenchantment Bay, Alaska: implications of recognizing marine jökulhlaup deposits in the stratigraphic record. Mar. Geol. 284, 1–12.
Yde, J.C., Knudsen, N.T., Hasholt, B., Mikkelsen, A.B., 2014. Meltwater chemistry and solute export from a Greenland ice sheet catchment, Watson River, West Greenland. J. Hydrol. 519, 2165–2179.
Zhao, Y., Gao, G., Ding, G., Zhou, Q., Zhang, Y., Wang, J., Zhou, J., 2022. Improving the performance of an unmixing model in sediment source apportionment using synthetic sediment mixtures and an adaptive boosting algorithm. Catena 217, 106491. https://doi.org/10.1016/j.catena.2022.106491.